university of groningen

faculty of mathematics and natural sciences

Varying constants and the search for physics beyond the Standard Model

Abstract: precise calculations on two sets of molecules are performed to determine their sensitivity to changes in the fine structure constant and the proton-to-electron mass ratio. Variations in these fundamental constants might provide clues as to what lies beyond the Standard Model. CC and CI methods are used up to CCSD(T) level and d-aug-dyall.v4z basis sets. Absolute enhancement factors up to 4×10^3 cm^{-1} for α and -1×10^5 cm^{-1} for μ are reported. The Cl_2^+, O_2^+, Ge_2^+ and As_2^+ molecules are advised strongly for experiment.

Masters' Thesis Physics

Juli 2017

Student: J. H. A. Ellen, s2214962

Primary supervisor: Prof. Dr.A. Borschevsky

Secondary supervisor: Prof. Dr. R. Havenith

Contents

1 Introduction

Since its inception in 1962, the Standard Model of physics has proved its worth over and over again, predicting with great precision the existence of particles and their decay chains. The most notable feat would be the discovery of the Higgs boson in 2012, which was first predicted almost fifty years prior [1]. But also a more recently observed decay of the strange B meson shows a striking agreement with predictions [2]. The Standard Model is an attempt to create a "theory of everything", combining all knowledge of physics in a single idea. The principle that keeps this idea together is the Standard Model Lagrangian, which describes the interactions of fermions and bosons. Since all matter is build up from those particles, the Standard Model describes everything around us. Despite its overwhelming success, the Standard model is not truly a "theory of everything" but rather a "theory of *almost* everything". Although the Standard Model Lagrangian describes the interactions of the fundamental particles, it only takes three of the four physical forces into account, namely the strong, the weak and the electromagnetic force. This immediately shows that the Standard Model (SM) is incomplete, since it fails to incorporate the gravitational force. Other problems of the SM are that it can not explain the existence of dark matter [3], the matter-antimatter asymmetry [4] and the fact that neutrino flavor oscillations prove that they are not the massless particles the Standard Model predicts them to be [5].

Several extensions that solve the shortcomings of the Standard Model have been proposed. These include minor modifications, such as implementing a mechanism to give mass to neutrinos [5, 6], as well as major revisions, such as string theories [7]. Supersymmetry for example, may solve the dark matter problem by introducing a heavy superpartner of all known particles [8]. Many of these theories belong to a class of theories called Grand Unification Theories (GUTs) [9, 10, 11]. The basic idea of these theories is that the Standard Model is part of a larger symmetry group. In this grand symmetry the fundamental forces (with or without gravity depending on the theory) are indistinguishable. The Standard Model as we know it then arises when this grand symmetry is spontaneously broken. This spontaneous symmetry breaking would occur at a cutoff energy much larger than the energies we encounter in every-day physics [11].

Theories for physics beyond the Standard Model may produce predictions by which they can be verified. A prediction may be a new particle or force, which could then be a dark matter or dark energy candidate [3]. Alternatively the new physics might provide an explanation to the matter-antimatter asymmetry [10, 12]. Predictions like this are tested by attempting to produce the predicted particles, for example at particle accelerators like the Large Hadron Collider. A GUT might also allow fundamental constants to vary over time and/or space [13]. This variation would be heavily suppressed at our everyday energy scale but could be measured in an experiment. This would allow for a verification of the theory.

For this work research into the variation of the fundamental constants is of particular interest. Therefore it is useful to take a closer look at what separates an ordinary constant from a fundamental one.

A fundamental constant is a constant that takes a specific value to make a theory consistent with observations. Their values are not predicted by the theory they are part of and thus will have to be measured. Therefore they will never be known exactly, as there is always some uncertainty involved with a measurement. This could also cause fundamental constants to 'change' as new, more accurate experiments are being performed. The improvement of measurement techniques is not the only way a fundamental constant can change. Another possibility is that a fundamental constant is 'explained', proven to be a natural outcome of a larger theory. A fundamental constant is only as fundamental as the theory it is part of!

An example would be the gravitational constant g, the acceleration due to gravity on Earth.

For many centuries this was a fundamental constant, since there was no underlying theory to explain its value. Then Isaac Newton came along and introduced the concept of forces and the laws they obey. His formula for the attractive force of two bodies is shown below:

$$F = G\frac{m_1 m_2}{r^2} \tag{1}$$

Using the mass and radius of the Earth quickly gives the constant g we are familiar with, but in the greater scope of things it is replaced by G. Newton *unified* gravity by showing that it is more widely applicable than previously assumed. By showing that g is not universal, nor a constant, physicists were required to alter their understanding of the fundamentals of physics and to include a gravitational force with its own fundamental constant G. In the early 20^{th} century, gravity was unified with the larger theory of general relativity by Einstein, proving once more that the status of 'fundamental constant' is temporary at best.

So if we were to discover a change in a current fundamental constant it would provide more evidence that our current understanding of the world around us is incomplete. The list of constants that are currently under scrutiny is quite extensive, including: the deuterium binding energy B_D, the proton-neutron mass difference Q_{np}, the lifetime of the neutron τ_n, the proton to electron mass ratio μ and the fine structure constant α [14].

The two fundamental constants of which the possible variation is the focus of this thesis are the proton-to-electron mass ratio $\mu = \frac{m_p}{m_e}$ and the fine-structure constant $\alpha = \frac{e^2}{\hbar c}$. The first stems from the coupling of the strong force, which determines a large part of the proton's mass [15, 16] and the second plays a major role in the coupling of the electromagnetic force. Throughout this work I will use atomic units ($e=\hbar=m_e=1$). Detecting a variation of the fundamental constants is highly nontrivial since if they change at all, they change very little [14].

Over the years, many experiments have been performed in the search for variation of fundamental constants. Using the most modern and accurate atomic clocks, the rate of change of both α and μ is determined to be at most -0.7± 2.1 × $10^{-17} yr^{-1}$ and -0.2± 1.1 × $10^{-16} yr^{-1}$ respectively [17]. These results are consistent with zero variation. If we want to further constrain the bounds on these rates of change the precision of our experiments will need to be increased.

The goal of this thesis is to facilitate new experiments by providing accurate information on molecular transitions which happen to be very sensitive to changes in α and μ. To this end the spectroscopic properties of various molecules are determined by performing state-of-the-art *ab initio* calculations. The values of these properties will be the most precise ones to date. Using this information the sensitivity of the transitions to variations of the fundamental constants of these molecules may be determined. Combining the newest technology with hand-picked, sensitive transitions may just provide the information needed to enter a new era of physics beyond the Standard Model.

2 Search for the variation of fundamental constants

Since the possible detection of a variation of the fundamental constants could make new physics necessary, the search for any change has been ongoing for many years [18, 19]. It is often not possible to measure a fundamental constant directly. They are made to be dimensionless and a measurement will always give a result in volts, currents or other observable quantity. If a fundamental constant would be measured the error in the units of the constant would dominate the uncertainty.

The observable by which we measure a change in a fundamental constant may be heavily dependent on a physical framework. When for example investigating the variation of the fundamental constants using the Cosmic Microwave Background (CMB) or supernovae, cosmological

models will always be involved [20, 21]. Thus it is important to find a balance between lookback time, precision and 'directness'.

The lookback time is how far in the past the baseline measurement was, and thus how much time we have given a fundamental constant to change before it is re-probed. This is important because the current upper limit on the variation of α and μ is on the order of $10^{-17}yr^{-1}$. Astronomical observations at high redshift have a large lookback time, but usually are lower in precision [22].

Precision is what can make up for a short lookback time. In principle it should be possible to measure a variation as the years pass if the accuracy of $10^{-17}yr^{-1}$ can be obtained. This level of precision can only be reached if the investigated system is sensitive to the variation. Finding which atoms and molecules are sensitive is not at trivial task, however.

Directness is an issue which is always present in experimental physics. The problem is that all measurements are performed in a certain theoretical framework and not all results can be separated from this framework [23]. This means that uncertainty or bias in a theoretical frame will influence the reliability of the results. The less a measurement depends on the theoretical model, the more direct it is.

All experiments up to this point are consistent with no variation. In the rest of this chapter I will give a short overview of experiments that are being or have been performed in the field, focusing on the constants that are of most interest to this thesis, α and μ.

2.1 Oklo natural reactor

In 1972, at a nuclear enrichment facility in France, a sample of uranium ore from the Oklo uranium mine in Gabon was tested. It turned out that the ratio of the uranium isotopes $^{235}U/^{238}U$ was lowered from the usual 0.7% to about 0.6% [24]. Since uranium can be used to produce atomic weapons further research was instigated. The result of this inspection was that natural fission occurring approximately 2 billion years ago was the cause for the uranium depletion in exactly the same way it would happen in a present-day reactor.

Neutrons produced during fission reactions are too high in energy to continue the chain reaction. In a present-day reactor the neutrons would need to be slowed down (moderated) to increase the interaction cross-section to the point at which the process can sustain itself. Groundwater that happened to be present at the Oklo site 2 billion years ago served the purpose of moderating the reaction. This allowed the whole system to behave just like a modern reactor would today. The slowed neutrons were captured by minerals in the groundwater, changing their isotope ratios. The quantity of these minerals and their isotope contents can be accurately determined today [24].

Some of those minerals are particularly good at capturing neutrons due to certain thermal resonances. An example of a such a mineral is Samarium (^{149}Sm), which, upon capturing a neutron, becomes ^{150}Sm. It was found that the amount of ^{149}Sm was depleted due to the absorption of neutrons. Since the neutron flux at the time of the fission is relatively well known, as well as how many absorptions must have taken place, it is possible to put bounds on the interaction cross-section. It so happens that this cross-section is heavily dependent on the fine-structure constant α, as was first shown in [19]. Thus, knowing what its value must have been in the past to account for the observed amount of ^{149}Sm, a bound can be put on the variation of α. In 1996, the upper limits of this variation were determined to be [25]:

$$-6.7 \times 10^{-17} < \frac{\dot{\alpha}}{\alpha} < 5.0 \times 10^{-17} yr^{-1} \tag{2}$$

The most recent limits were set in 2015 [26]:

$$\frac{\dot{\alpha}}{\alpha} < 5 \times 10^{-18} yr^{-1} \tag{3}$$

With this result the Oklo natural reactor provides the most stringent limit to date in the search for the variation of fundamental constants.

2.2 Atomic clocks

An atomic clock is a device that tracks time by counting periods of radiation. The radiation comes from an electronic decay in the energy structure of an atom. This method has proven to be so accurate that the second is actually defined as [27]:

The duration of 9192631770 periods of radiation belonging to the two levels of hyperfine splitting of the Caesium-133 ground state

Since the energies of the hyperfine levels depend on fundamental constants such as the fine structure splitting and the electron-to-proton mass ratio a variation in the latter two would alter the length of a second. The dependence of the hyperfine frequency of alkali-like atoms (such as the commonly used ^{133}Cs) on the fundamental constants looks like [14]:

$$\nu_{hfs} \approx R_\infty c \times A_{hfs} \times g_i \times \alpha^2 \times \mu^{-1} \times F_{hfs}(\alpha) \tag{4}$$

Here R_∞ is the Rydberg constant, A_{hfs} and g_i depend on the used atom, μ is the electron-to-proton mass ratio and $F(\alpha)$ includes relativistic corrections. The factors that depend on the atoms serve the important role of making the system unique. It is *impossible* to check for a difference in a fundamental constant if you compare two clocks using the same transition to each other since they will change *identically* under the VFC. This is why experiments of this kind always compare two transitions that depend differently on the fundamental constants between two separate clocks.

Atomic clock experiments are very suited for the search for the variation of the fundamental constants since they are relatively low in maintenance and high in accuracy. The setup is simple: build two (or more) atomic clocks based on different atoms and note the frequency difference in the measured transition while taking systematic errors into account [28]. Alternatively you can measure two different transitions in the same atom. If there is no change in the fundamental constants the rate of change of the frequency ratios is zero. Due to the simple experimental setup it is possible to monitor this change over several years. The downside to atomic clock experiments is that the observation time is very small compared to the timescale at which the variation of the fundamental constants would occur, so that very high precision is required. Additionally the atom-dependent constants in equation 4 bring a certain uncertainty with them since they too are experimentally determined [23].

Many atomic clock experiments are being performed all over the world. Since they are still are gathering data right now, precision is expected to improve as the years pass. At present the limit on the variation of the fine structure constant and the electron-to-proton mass ratio is set by comparing the frequencies of two transitions of $^{171}Yb^+$ in a single atom [17]:

$$\begin{aligned} \frac{\dot{\alpha}}{\alpha} &= -0.7 \pm 2.1 \times 10^{-17} yr^{-1} \\ \frac{\dot{\mu}}{\mu} &= -0.2 \pm 1.1 \times 10^{-16} yr^{-1} \end{aligned} \tag{5}$$

2.3 Quasar cloud absorption

The lookback times of the experiments described up until now have ranged from a few years for atomic clocks up to a few billion years in the case of the Oklo natural reactor. In cosmological terms one would say the redshift ranged from z=0 up to z≈0.14. On these timescales the fundamental constants will have varied very little (if they vary at all). Astronomical observations can probe redshifts up to z≈1000, the redshift of the Cosmic Microwave Background [14], making astronomical research promising for the search for the variation of the fundamental constants.

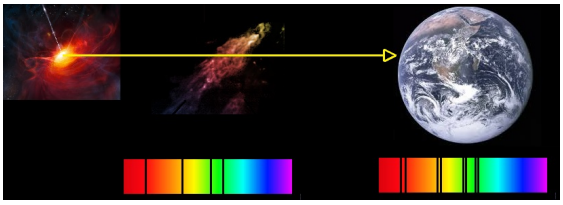

Figure 1: The principle of absorption spectra. Light from a distant quasar is absorbed by molecules in a dust cloud. If the fundamental constants changed as the light traveled from the cloud to Earth, the absorption lines are broadened or doubled.

Light from quasars, originating at a redshift between z=1 and z=7, is so bright that it can be used to perform spectroscopic measurements. For this kind of research it is required that the light passes through a gas cloud before reaching the Earth. Atoms in such a cloud absorb certain wavelengths of light, corresponding to their electronic transitions, which in turn depend on the fundamental constants. If a fundamental constant was different in the past, the spectral lines of atoms and molecules in a dust cloud would appear at a different wavelength than their present-day laboratory value. This method was first introduced by Savedoff in 1956 [29] and was used many times thereafter [30, 31, 32]. A schematic overview of the principle of analyzing gas spectra can be found in figure 1.

There are many uncertainty factors involved with using galactic gas spectra for research into the variation of the fundamental constants. Due to the redshift induced by the expanding universe, one can not compare the incoming spectrum with one obtained in a laboratory directly. To compensate for the redshift ultimately one must choose some cosmological model [21]. In addition, assumptions about the abundance of certain elements in galactic dust clouds must be made. Also there are large uncertainties in measuring the differences in transition energies. To illustrate: a change in α on the order of 10^{-5}, which is much larger then the current upper limits, is only a third of a pixel of an imaging device as used in the experiments in this field [14].

Luckily redshifting, which would otherwise be a large factor of uncertainty, is a chromatic effect, i.e. it acts the same on all wavelengths. This allows for the separation of the redshift from the possible variation of fundamental constants. This works because the latter affects some wavelengths differently than others. The following formula is used to determine how a measured change in transition frequency is caused by a change in the fine-structure constant α [33]:

$$\omega = \omega_0 + q\left[\left(\frac{\alpha}{\alpha_0}\right)^2 - 1\right] \tag{6}$$

Here ω_0 is the transition frequency in the laboratory, ω is the transition frequency in the cloud at redshift z. α_0 and α are the fine-structure constants now and at redshift z respectively. The q factor determines the sensitivity of the transition to a possible variation of the fundamental constants. The q factor can be computed using the same techniques as will be applied later in this work and are also useful for the atomic clock experiments discussed earlier.

A variety of observations using many different methods (e.g. Alkali Doublets, Many Multiplet, Single Ion Differential Measurement) have been performed on several atoms and small molecules (e.g. H, O, NH_3) [14]. In 1999 Webb et. al. obtained a nonzero limit on the variation of α [30].

This result was obtained by analyzing 30 absorption systems of 17 quasars from a Keck/HIRES data set. Expansions on this research including more absorption spectra confirmed this result [22]. In 2004 however, Chand et. al. [34] found another result when analyzing a smaller, but more strict data set from the VLT/UVES telescope. This result was again consistent with no variation of the fundamental constants. Webb et. al. then claimed to have improved the statistical analysis of that data set so that the null constraint on the variation of α found in [34] was no longer significant [35]. This controversy shows just how important rigorous analysis is when searching for such minute differences.

More recently, Webb et. al. released an analysis of a data set of the VLT and the Keck telescopes, which showed that α increases in one direction in space and decreases in the other [36, 37]. This dipole effect was reported to have a significance of 4.2σ. In a later paper, Berengut and Flambaum discuss how laboratory experiments may be interpreted in the light of α varying in space, and maybe also in time [38]. The existence of a dipole variation of α is still heavily disputed, with a recent paper again publishing a null constraint on its variation [39].

The values of the variation of the proton-to-electron mass ratio μ are still consistent with a null constraint as was shown in recent studies of alcohol [40] and hydrogen [41] spectra. Two of the most conservative limits on the difference of α and μ with respect to their present values are given below, obtained from [39] and [41] respectively. Note that these are integrated variations, i.e. the difference in alpha at the cloud's redshift and our current alpha. Previously the variation was given as a rate of change per year.

$$\begin{aligned} \frac{\Delta\alpha}{\alpha} &= (0.01 \pm 0.26) \times 10^{-5} \\ \frac{\Delta\mu}{\mu} &= (0.0 \pm 1.0) \times 10^{-7} \end{aligned} \tag{7}$$

2.4 Molecular transitions

Rather than measuring atomic transitions, which is the case in atomic clocks, one can also perform precise measurements on molecular transitions. In atomic clock experiments in the optical regime, only the variation of the fine structure constant α can be probed. One of the advantages of using molecules over atoms is that the energy levels are always sensitive to changes in the proton-to-electron mass ratio μ, as well as to the fine structure constant α [17]. In addition to this, molecules also display additional structure such as rotational and vibrational splitting, Λ-doubling, fine structure and forbidden/enhanced transitions [42]. All of these depend differently on the fundamental constants, allowing for a detailed comparison if enough data can be gathered.

Despite the advantages, only a few molecules have been used for molecular clock experiments up until now, examples being OH and SF_6 [43] [44]. This is because slowing and trapping the right molecules for this kind of measurement has only recently become possible [42]. Prospective experiments look for transitions that display enhanced sensitivity to the variation of the fundamental constants in their subject molecules. Especially transitions between quasi-degenerate energy levels that depend differently on the fundamental constants are very suited for this type of research. This is because the enhancement of the sensitivity of a transition to the variation scales as $\delta\omega/\omega$, which tends to infinity as the transition frequency $\omega \to 0$. In order to identify these favorable transitions much research has been done using highly precise *ab initio* computer calculations. Possible candidate molecules are: I_2^+ (and a wide variety of other dihalogens) [45], Cs_2 [46], NH^+ [47], Sr_2 [48] and SiBr [49, 50]. Identifying favorable transitions in a variety of molecules is an open field with great prospects for the future. High precision experiments are heavily reliant on this theoretical research. This is why I, too, will dive into the the field of finding clues as to what lies beyond the Standard Model.

3 Research goals and outline

The goal of this work is to predict which (if any) molecules out of a given set have electronic transitions are sensitive to a variation of the fundamental constants. With this information new experiments could be set up that use a particularly sensitive molecule to narrow down the limits on the variation even further. In this sense this work is a continuation of the work done in [45] and [50].

The group of molecules that will be investigated in this work consists of: Ge_2^+, As_2^+, Sn_2^+, Sb_2^+, C_2^+, O_2^+, S_2^+, Cl_2^+, SeO^+, $SiSe^+$, $SiTe^+$, SO^+, TeO^+ and PbS^+. They will be treated in two groups. The molecules were selected by comparing their transition energies to their harmonic constants. If one is a multiple of the other then they are expected to have quasi-degenerate levels, which is an indication of sensitivity to the variation of the fundamental constants. An additional reason to investigate these molecules in particular is that they are all ionic, which will make them easier to manipulate in an experiment.

A transition is sensitive if three conditions are met. To start the molecule should be inherently sensitive to variations in the fundamental constants. Additionally, the transition should take place between quasi-degenerate levels, as can be seen from the $1/\omega$ dependence of the enhancement factors. A last requirement is that the energy levels of the transition behave differently under the variation of the fundamental constants. If the energy levels display a similar dependence no net change will be measured in experiment. This principle is also illustrated in Figure 2. The most optimal scenario would be that the levels move oppositely to each other so that the relative change is large.

To predict whether a transition is sensitive we look at the enhancement factors of this transition. These are a measure of the degree to which the transition is dependent on the fundamental constants and thus of how much it is expected to change if they do. In equation 8 the relative sensitivity of the transition frequency is given as a function of a change in the fundamental constants, multiplied by their enhancement factors K_μ and K_α [45]. These factors describe the sensitivity to variation of α and μ respectively.

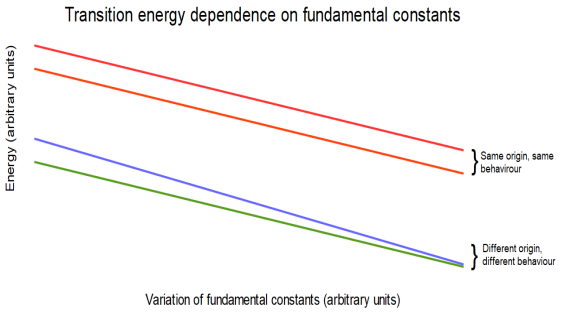

Figure 2: Top: no net difference if both levels vary identically if the fundamental constants change. Bottom: if the levels are of different origin, a net difference can be measured.

$$\frac{\delta\omega}{\omega} = K_\mu \frac{\delta\mu}{\mu} + K_\alpha \frac{\delta\alpha}{\alpha} \tag{8}$$

The enhancement factors themselves are functions of the spectroscopic constants of the molecules and are inversely proportional to the transition frequency. They are shown in equation 9. A detailed derivation will be given in chapter 5.

$$\begin{aligned} K_\mu =& \big[\frac{1}{2}\omega_e(\nu_2-\nu_1) - \omega_e x_e(\nu_2-\nu_1)(\nu_1+\nu_2+1) \\ &+ B_e(J_2-J_1)(J_1+J_2+1)\big]\omega^{-1} \\ K_\alpha =& \frac{\delta T_e}{\delta\alpha}\alpha_0\omega^{-1} \end{aligned} \tag{9}$$

The spectroscopic constants are a measure of the inherent sensitivity of a molecule and can be experimentally determined. From the fact that the enhancement factors scale inversely with

ω the importance of quasi-degenerate levels becomes clear. The $\frac{\delta T_e}{\delta \alpha}$ factor in the expression for K_α is only known analytically for fine structure transitions. This poses some difficulties for some of the molecules, but using calculations the factor can be determined directly.

Although the spectroscopic constants should be obtained from experiment, this data is not always available. This leads to natural split of the initial molecule set into one for which the spectroscopic constants are not known and one in which they are. The first group of molecules consists of Ge_2^+, As_2^+, Sn_2^+, Sb_2^+, SeO^+, $SiSe^+$, $SiTe^+$, SO^+ and TeO^+. The second is formed by C_2^+, S_2^+, SO^+, Cl_2^+ and O_2^+.

The missing spectroscopic constants of the first group were be obtained from their potential energy curves using a computer program. The curves themselves have been calculated using the very precise relativistic coupled cluster method (CC) [51]. An example of such a curve is given in Figure 3. Since their shape is directly related to the spectroscopic constants, the potential energy curves of the second molecule group were already known.

Reconstructing the potential energy curves is important because it makes looking for quasi-degenerate levels more easy. The most sensitive transitions take place between carefully selected vibrational and rotational levels. By drawing the vibrational levels into the energy curves, as was done in figure 3, it is possible to select the quantum numbers that belong to quasi-degenerate levels.

After selecting the quasi-degenerate vibrational states we can add the rotational levels on top of the rotational ones. This brings the energy gap from $\sim 10 cm^{-1}$ to less than an inverse cm. An example of the rotational levels belonging to the transition that is indicated in Figure 3 is included in Figure 4. Since the spectroscopic constants of the second molecule group are known, the favorable transitions had already been identified using the same tools.

For the first molecule group only fine structure transitions were investigated. This, among other things, allows for a fully analytic expression of equation 9. The second molecule group also includes electronic transitions, however, for which this is not the case. This means that the $\frac{\delta T_e}{\delta \alpha}$ factor had to be calculated directly. This has been done by calculating

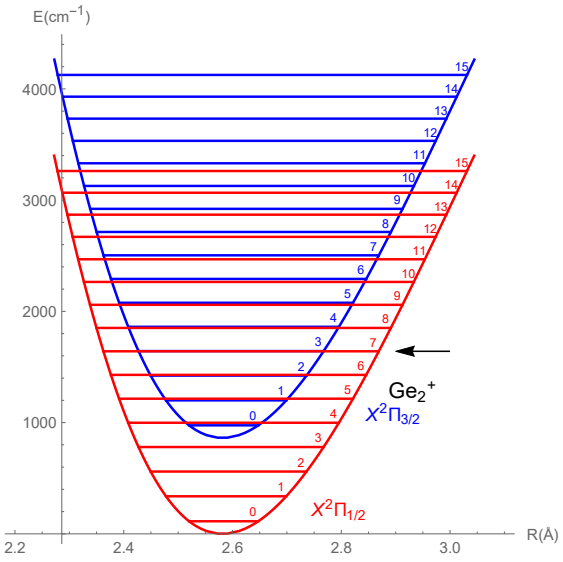

Figure 3: Potential energy curves of the substates of the $X^2\Pi$ state of Ge_2^+. Horizontal lines indicate the quantized vibrational levels, with an arrow pointing to a quasi-degenerate transition.

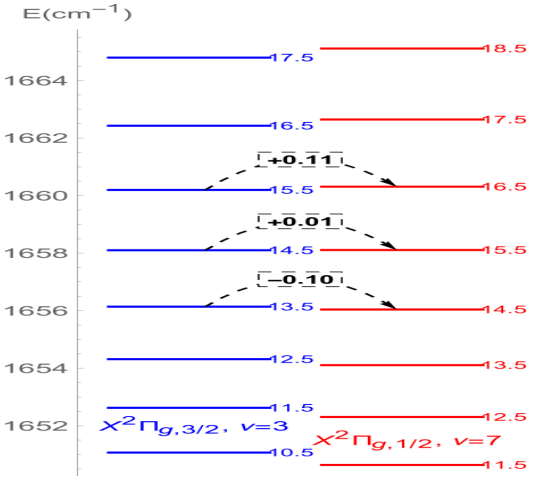

Figure 4: Rotational levels on top of the $\nu = 3$ and $\nu = 7$ vibrational levels of the fine structure of Ge_2^+. Quasi-degenerate transitions and their separation have been indicated.

the electronic transition energy T_e for several values of α. This calculation was performed using the configuration interaction (CI) [52] method.

It should be clear that precise calculations are the key in predicting which transitions are sensitive to the variation of the fundamental constants. The calculations can be used to provide the spectroscopic constants needed to determine if the high inherent sensitivity and quasi-degenerate transitions that are necessary for favorable transitions are present in a molecule. It is for this reason that the next chapter is dedicated to understanding the various components that make a calculation precise.

The techniques of chapter 4 are then used to investigate the molecules using the appropriate calculational methods. The detailed description of this research is given in chapter 5, as well as the resulting enhancement factors. The obtained results will be discussed in chapter 6.

4 Computation methodology

Since experimental data is unavailable for most of the molecules in the first group we must resort to the second best option: accurate calculations. The goal of the calculations is to obtain the spectroscopic constants of these molecules with the highest possible precision, which in turn means that we need to accurately determine the shapes of their potential energy curves. The need for high precision means that we must also take relativity into account. Since α is related directly to the speed of light it is mainly important in the relativistic regime. It is the dependence on the fine structure constant that makes fine structure an inherently relativistic effect.

There are many factors that influence the precision of calculation, most of which are within control of the user. However, one must always keep in mind that any increase in precision leads to an increase in calculational complexity and thus in computational cost.

When performing a calculation we set out to solve the time independent Schrödinger equation:

$$\mathbf{H}\,|\Psi\rangle = E\,|\Psi\rangle \tag{10}$$

This means finding the wave-function Ψ of the complete system and the corresponding energy eigenvalue E for a suitable choice of the Hamiltonian $\mathbf{H}$. Already we see two variables that could be controlled: $\mathbf{H}$ and Ψ. Both of these parameters are often too complex to be included exactly. Choosing the right approximations is one of the greatest challenges of molecular orbital calculations.

In general the quality of a calculation is determined mostly by the following three parameters.

- Inclusion of relativity, determined by the choice of Hamiltonian
- Degree to which electron-electron interaction is taken into account (electron correlation)
- Flexibility in the description of the wavefunction (basis set)

To obtain the exact energy of a system one must include all three parameters to their full extent. Given our current computation power getting close to this exact energy is only possible for systems of up to a few electrons. In order to control the degree to which the three parameters are included computational methods come in packages. These packages contain a variety of Hamiltionians, several correlations schemes and many basis sets. This allows us to perform our calculations at the level of precision we require while still being feasible within the resource limits. I used the DIRAC15 package [53] since it is set up to handle relativistic calculations but many more are available (see for example [54] and [55]). The rest of this chapter will explain the influence of the three parameters in detail and introduce the methods I used.

4.1 Relativity

The inclusion of relativity is especially important when a specific relativistic effect is investigated (which is the case for the fine structure splitting) or when the system is heavy [56]. Due to special relativity electrons moving at speeds close to the speed of light appear to be much heavier then their slow-moving classical counterparts. The heavy electrons move on orbits closer to the nucleus, where they are more tightly bound. Shells with low angular momentum (s, $p_{1/2}$) are contracted and stabilized more then those with higher angular momentum ($p_{3/2}$, d, f) due to the latter experiencing a centrifugal barrier. Not only are d and f shells not contracted, they are even destabilized by the changes to the orbitals in the s shell.

Aside from the changes to the orbitals, relativity also causes degenerate levels to split. This is caused by the magnetic moment induced by the electron's trajectory, which couples to the electric field surrounding the nucleus. This spin-orbit effect is different for electrons with different angular momentum within a shell, causing the energy levels to split.

A Hamiltonian describing a relativistic system should take the various effects into account, which is usually accomplished by modifying a non-relativistic Hamiltonian. The standard form of a Hamiltonian in the Born-Oppenheimer approximation is given in equation 11 [57]. In the Born-Oppenheimer approximation the nucleus is regarded as stationary, which has proven to be very accurate due to the large mass difference between the nucleons and the electrons. Although there are many Hamiltonians available, including various degrees of relativity, all of them are of the form given in equation 11 .

$$\mathbf{H} = \sum_i \hat{h}(\mathbf{r}_i) + \frac{1}{2}\sum_{i,j} \hat{g}(\mathbf{r}_i, \mathbf{r}_j) + V_{NN} \tag{11}$$

The first term in the Hamiltonian consists of the one-electron operators for electrons located at $\mathbf{r}_i$, i.e. the energy from the attraction between the electrons and the nucleus as well as the energy associated with their kinetic energy. The dimension of this operator determines the degree to which relativity has been taken into account. In the non-relativistic case, it is a scalar operator. In the the fully relativistic case it is given by the relativistic one electron Dirac Hamiltonian [57]:

$$\hat{h} = c\alpha \cdot \mathbf{p} + mc^2\beta + V \tag{12}$$

Which is a (4×4) matrix and includes both the electron and positron, as well as their spins. Here α and β are Pauli matrices and $\mathbf{p}$ and V are the linear momentum and nuclear potential respectively. Note that in this case $\mathbf{p}$ is the relativistic 4-momentum. Computing the energies of a system using the fully relativistic, 4-component Dirac matrices may increase the required computational cost by two orders of magnitude [57]. In an effort to reduce the required computational resources several intermediate two-component Hamiltonians have been developed. In a two-component Hamiltonian the degrees of freedom of the positronic part of the Dirac matrices are frozen, leaving just the electrons to be considered. In my work I used the exact, two-component X2C Hamiltonian, which can almost exactly reproduce the electronic part of the fully relativistic Dirac Hamiltonian but at a lower computational cost [58, 59].

The second term in the Hamiltonian is the two electron interaction operator taken in its non-relativistic form. This term should take all interactions between the electrons into account. Since this multi-electron problem is very hard to solve, many schemes to include the electron correlation have been developed. These schemes will be discussed in more detail in the next section. The last term includes interactions between nucleons. In the Born-Oppenheimer approximation this interaction term can be considered to be constant for a certain bond distance, since this distance is changing much more slowly then the electronic interactions.

4.2 Correlation

The molecules we are dealing with contain tens of electrons and should thus be treated as many-body systems. In principle we would like to include all interactions between all individual electrons at any given moment in our calculations. In reality this is not feasible due to the large number of interactions one would need to take into account. The degree to which the instantaneous interactions between individual electrons is considered is called *electron correlation* [60]. When performing a calculation one needs to include electron correlation in such a way that the results are both precise and computationally feasible.

There are many interaction schemes, with varying degrees of correlation [52, 61]. One of the most straightforward models is the Hartree-Fock (HF) method, which was first proposed in 1930. In the HF method electron correlation is ignored and the electrons are only affected by an averaged force originating from the electron cloud surrounding them. This leads to alternative definition of the degree of correlation, namely the difference between the energy according to the HF method and the fully correlated 'true' energy [60].

Since the HF method is relatively low in computational costs it is often used as a starting point for more elaborate correlation schemes. Therefore I will treat it in more detail below. The rest of the section deals with the two major correlation schemes I used in my research, the configuration interaction [52] and the coupled cluster [61] methods.

4.2.1 The Hartree-Fock method

We wish to find a total wavefunction that describes all electrons. As a starting point , let's look at the one electron Schrödinger equation:

$$\hat{h}(\mathbf{r})\phi_0(\mathbf{r}) = E_0\phi_0(\mathbf{r}) \tag{13}$$

In the simplest approximation to the total energy we neglect electron interaction altogether ($\hat{g} = 0$ in equation 11). In this case the electronic energy is due only to the potential of the nucleus, which makes equation 13 relatively easy to solve. Equation 13 holds for each individual electron and since interaction is neglected in the HF method the total wavefunction is simply the product of the one-electron wavefunctions:

$$\Psi = \prod_i \phi_i(\mathbf{r}_i) \tag{14}$$

Of course we do not want to treat electrons as non-interacting particles since not only does it not add anything to our solution, the situation is also unphysical. The most blatant error is that this total wavefunction would not obey the Pauli exclusion principle [62]. Instead we strive to create linear combinations of the one-electrons wavefunctions. These are obtained by computing the so-called *Slater determinant* for n electrons:

$$\Psi = \frac{1}{\sqrt{n!}} \begin{vmatrix} \phi_1(\mathbf{r}_1) & \phi_2(\mathbf{r}_1) & \phi_3(\mathbf{r}_1) & ... & \phi_n(\mathbf{r}_1) \\ \phi_1(\mathbf{r}_2) & \phi_2(\mathbf{r}_2) & \phi_3(\mathbf{r}_2) & ... & \phi_n(\mathbf{r}_2) \\ \phi_1(\mathbf{r}_3) & \phi_2(\mathbf{r}_3) & \phi_3(\mathbf{r}_3) & ... & \phi_n(\mathbf{r}_3) \\ \vdots & \vdots & \vdots & \ddots & \vdots \\ \phi_1(\mathbf{r}_n) & \phi_2(\mathbf{r}_n) & \phi_3(\mathbf{r}_n) & ... & \phi_n(\mathbf{r}_n) \end{vmatrix} \tag{15}$$

Here Ψ is the antisymmetric total wavefunction, which is obtained from the determinant of all permutations of the one-electron wavefunctions $\phi(\mathbf{r}_i)$, or orbitals. For example: the total wavefunction for a two-electron system obtained using the Slater determinant is given by:

$$\Psi = \frac{1}{\sqrt{2}}(\phi_1(\mathbf{r}_1)\phi_2(\mathbf{r}_2) - \phi_2(\mathbf{r}_1)\phi_1(\mathbf{r}_2)) \tag{16}$$

Which is as we expect from elementary quantum mechanics. Also note that using the Slater determinant to form a total wavefunction is consistent with the picture of indistinguishable electrons, which states that we can not say with certainty which electron occupies which orbital [62].

Although the HF method neglects instantaneous interactions, the one-electron wavefunctions are still influenced by the average fields induced by the presence of the other electrons. In the HF this is accomplished by replacing the Hamiltonian in the one-electron Schrödinger equation by the Fock operator [63]:

$$\hat{F} = \hat{h} - \sum_{j}^{n} 2\hat{J}_j - \hat{K}_j \tag{17}$$

Where $\hat{h}$ is still the one-electron operator from equation 11 and the $\hat{J}$ and $\hat{K}$ operators are defined by:

$$\begin{aligned} \hat{J}_j(\mathbf{r}_1)\phi_i(\mathbf{r}_1) &= \int d^3\mathbf{r}_2 \phi_j^*(\mathbf{r}_2)\phi_j(\mathbf{r}_2)\frac{1}{r_{12}}\phi_i(\mathbf{r}_1) \\ \hat{K}_j(\mathbf{r}_1)\phi_i(\mathbf{r}_1) &= \int d^3\mathbf{r}_2 \phi_j^*(\mathbf{r}_2)\phi_i(\mathbf{r}_2)\frac{1}{r_{12}}\phi_j(\mathbf{r}_1) \end{aligned} \tag{18}$$

So that the second part of equation 17 gives the averaged potential felt by the electron in question.

The electron we are solving equation 18 for is part of the potential for the other electrons. So in order to obtain a precise n-electron wavefunction we will need to solve the entire system iteratively. The steps are as follows [63]:

- Guess some reference Slater determinant, i.e. some set of wavefunctions $\{\phi_0\}$, and compute the total energy
- Solve equation 18 for each individual electron using these wavefunctions to obtain the Fock operator
- Solve the one-electron Schrödinger equation using the Fock operator
- Compare the total energy computed with the set of new wavefunctions obtained this way with the initial total energy
- If the new energy is significantly different, take the new set of wavefunctions as a new reference and repeat the process

This iterative process is called the *Self Consistent Field* method. The system is self consistent because the solution for an electron energy influences the effective potential for another electron, which in turn influences the first electron's energy. The result is a set of coefficients that determine which combination of wavefunctions yields a total wavefunction that minimizes the energy of the system. The wavefunctions that the total wavefunction can be constructed from is recorded in the basis set. The importance of a basis set will be discussed in more detail at the end of this chapter.

The HF method is very efficient, but not very precise. For this reason it is often used to compute a set of input wavefunctions for more advanced methods [62, 63]. Two methods that are often used and that I also used in my research will be explained in detail below.

4.2.2 Configuration interaction

The Hartree Fock method, although computationally efficient, gives an incomplete picture of the total wavefunction. If we wish to truly recreate a total wavefunction from the one-electron wavefunctions we can not restrict ourselves to a single set of orbitals (a single Slater determinant). If we include all possible Slater determinants, formed from all possible electron occupations of an infinite basis of orbitals, then the *exact* total wavefunction would be given by the sum of these determinants [64]. Of course, an exact total wavefunction would also incorporate any interaction force felt by the individual electrons. In order to obtain such an exact total wavefunction, one would need to take as many determinants into account as there are possible electronic configurations, which is not possible.

The configuration interaction method seeks to expand upon the Hartree Fock method by adding many, but not infinitely many, Slater determinants to the total wavefunction. The fundamental equation is:

$$\Psi = c_0\phi_0 + \sum_{i\neq 0} c_i\phi_i \tag{19}$$

The first part of the total wavefunction is a reference set of one-electron wavefunctions ϕ_0, which are usually obtained with the standard Hartree Fock procedure. The other determinants ϕ_i belong to the wavefunctions of other configurations (hence configuration interaction) than the ground state. A configuration is an excited state that is obtained by promoting an electron in the ground state to a virtual (empty) orbital. In the current computational limit this excitation can be done to single electrons or to electron pairs. Configuration interaction with only single excitations is known as CI singles (CIS) and CI with both single and double excitations is known as CI singles doubles (CISD).

The determinants that belong to the configurations are weighted by the c_i parameter, which may be variationally determined. The optimization of these parameters is computationally expensive when many configurations have to be accounted for. This means that one has to find a delicate balance between including enough configurations to obtain a precise wavefunction and keeping this number as low as possible to save computer resources. Configurations including valence electrons determine a larger part of a molecule's energy and thus should always be included. [64].

The degree to which electrons are correlated can be controlled in two ways in the CI method. Firstly, there is choice whether to excite electrons individually (low correlation) or in pairs (higher correlation). Secondly there is the choice as to which virtual orbitals the electrons should be excited to. Exciting only to the first few virtual orbitals introduces less degrees of freedom and is computationally cheaper. However, this results in a worse description of a real system, in which the electron wavefunctions are nonvanishing everywhere.

The configuration interaction method is the best method available if all possible Slater determinants are used. However, the Slater determinants themselves are not perfect because not all orbitals are available to the electrons (the basis set is finite). One speaks of 'Full CI' if all possible Slater determinants within a certain basis set are used for a computation [61]. Full CI obtains the best correlation precision for a given basis set, but is only computationally feasible for very small systems. A different method that can be even more precise than CI and is less demanding is the coupled cluster (CC) method. A more detailed description of that method is given below.

4.2.3 Coupled cluster

As said earlier, another powerful method to include correlation is the coupled cluster (CC) method. It is best used for calculations for which high precision is required, which makes it perfect for my research. The fundamental equation in CC theory is [61]:

$$\Psi = e^{\hat{T}}\phi_0 \tag{20}$$

In this equation Ψ is the exact many-electron wavefunction and Φ_0 is the nonrelativistic HF ground state. The *correlation operator* is given by $e^{\hat{T}}$ and is defined by its Taylor expansion [65]:

$$e^{\hat{T}} \equiv 1 + \hat{T} + \frac{\hat{T}^2}{2!} + \frac{\hat{T}^3}{3!} + ... = \sum_{k=0}^{\infty} \frac{\hat{T}^k}{k!} \tag{21}$$

$$\hat{T} \equiv \hat{T}_1 + \hat{T}_2 + ... + \hat{T}_n \tag{22}$$

Here $\hat{T}$ is the *cluster operator*. It consists of the *one-particle excitation operator* $\hat{T}_1$, the *two-particle excitation operator* $\hat{T}_2$ etc. up to the maximum number of excitable electrons n. As an example $\hat{T}_1$ and $\hat{T}_2$ are given explicitly:

$$\hat{T}_1\phi_0 \equiv \sum_{a=n+1}^{\infty} \sum_{i=1}^{n} t_i^a \phi_i^a \tag{23}$$

$$\hat{T}_2\phi_0 \equiv \sum_{b=a+1}^{\infty} \sum_{j=i+1}^{n} \sum_{i=1}^{n-1} \sum_{i=1}^{n} t_{ij}^{ab} \phi_{ij}^{ab} \tag{24}$$

The result of the action of a particle excitation operator is that the ground state wavefunction is expressed as a linear combination of determinants in which electrons have been excited. In state ϕ_i^a electron i has been excited to virtual orbital a. In state ϕ_{ij}^{ab} a pair of electrons coming from orbital i and j have been excited to the virtual orbital pair ab. The higher order particle excitation operators look similar to $\hat{T}_1$ and $\hat{T}_2$. The t factors are similar to the weighting parameters we encountered in the CI method.

The result of applying the correlation operator $\hat{T}$ is that the ground state is expanded as a combination of excited states. If all excitation operators $\hat{T}_n$ are included within a given basis set we end up in the same regime as Full CI [65]. We already saw that Full CI yields the best total wavefunction for a given basis of orbitals. This makes the CC and CI methods very similar in the sense that they can both approach the exact wavefuntion for small systems.

The difference between the two methods lies in the computational resources required. For example CC with $\hat{T} = \hat{T}_1 + \hat{T}_2$, so that only excitations in singles and pairs are included, already has about the same precision as CISDTQ (CI up to quartet excitations). Yet it scales only as N^4n^2 instead of N^6n^4. Here n is the number of occupied orbitals and N is the number of virtual orbitals [61]. This is mainly due to the fact that it is much more computationally efficient to work with exponential operators, as is the case with CC.

I just mentioned CCSD, for which $\hat{T} = \hat{T}_1 + \hat{T}_2$. As is the case with CI, not all electron excitations are included due computational efficiency. The largest term in the series in equation 21 is $\hat{T}_2$. A CC scheme using only this term is known as CCD (coupled cluster doubles) [65]. The $\hat{T}_2$ term excites electrons 2 at a time in one pair, two pairs, etc. More precise schemes include more possible correlations. The current limit on the CC method as implemented in the DIRAC15 package is the inclusion of three terms of the cluster operator. This last term is only added approximately within perturbation theory. This method is known as singles, doubles and perturbative triples: CCSD(T), with the T in brackets to indicate its perturbative origin.

Although there are several schemes to add the triple excitations as a perturbation, CCSD(T) is commonly used and also the one I employed whenever possible.

When only a single determinant (usually obtained from the HF procedure) is used as a starting point for CC computations, the method is known as *Single Reference* coupled cluster (SRCC). Since this method uses only a single determinant it is only useful for states that are well described by this single determinant, such as the ground state and some low-lying excited states. Another method would be *Multi Reference CC* (MRCC) or *Fock Space CC* (FSCC) coupled cluster, in which more than one reference determinant is chosen. The second method is especially useful when the system has open shells or when transition energies are calculated [61], which is exactly what I was looking for in the first molecule set.

In principle one would always want to use MRCC for computations, considering its usefulness in computing transition energies. The method has two major downsides however. Firstly there is the fact that MRCC operates on the CCSD level of precision, whereas SRCC reaches the CCSD(T) level. This is because triple excitations for MRCC are simply not yet implemented in the DIRAC15 package, so the issue should be resolved with time. Additionally MRCC needs a closed shell system as input and at most two electrons can be added to the system or can be removed from it. This means that the method is only viable when the desired state is within two electrons of a closed shell system. For example, this is not the case for the second group of molecules, so I used CI rather then CC in those cases. Again this issue could be resolved by implementing the proper procedures into the DIRAC15 package and is thus not a fundamental limit.

4.3 Basis sets

The programs that compute the atomic and molecular properties use a basis set to define the orbitals the electrons move in. The basis set consists of many basis functions, which are one-electron wavefunctions. [60]. The goal is to reproduce the orbitals of an atom or molecule using linear combinations of these basis functions. If a basis set was complete (contained an infinite number of basis functions) the only error in the energy obtained from the HF procedure would be due to the approximated Hamiltonian. This 'ideal' energy is known as the *Hartree-Fock limit*. The discrepancy between the HF limit and the calculated energy is known as the *basis set truncation error*. Another way to phrase the goal of finding the optimal basis set is then that we want to minimize the basis set truncation error.

The types of basis functions discussed in this section are all atomic orbitals (AOs). When doing calculations on molecules the molecular orbitals (MOs) are determined by constructing a linear combination of atomic orbitals. In the HF procedure the energy of the molecule is minimized by finding the right coefficients in this linear combination.

Slater type orbitals (STO) try to mimic actual atomic orbitals using the spherical harmonics as their starting point. Making a complete basis out of them is computationally impractical. Additionally they are not always orthogonal to each other and predict zero amplitude in the nucleus for ns-orbitals with n>1 [60]. They are of the form:

$$\Psi_{nlm}(r,\theta,\phi) = Nr^{n-1}e^{-Z\rho/n}Y_{lm_l}(\theta,\phi) \tag{25}$$

where N is a normalization factor, n is the effective principle quantum number, $\rho \equiv r/a_0$ and $Y_{lm_l}(\theta,\phi)$ are spherical harmonics. By fitting equation 25 to calculated wavefunctions the orbitals may be optimized.

Gaussian type orbitals (GTO) obey convenient multiplication rules that are an inherent property of Gaussian functions. This increases the computation efficiency, but yields wavefunctions

that are not as similar to real orbitals as STOs. Gaussian orbitals are of the form:

$$g_{ijk}(\mathbf{r}) = Nx^i y^j z^k e^{-\alpha r^2} \tag{26}$$

Where N is a normalization factor, x, y and z are the coordinates of the nucleus and i, j and k are non-negative integers. Here α is a positive parameter, not the fine structure constant. Imposing addition rules on the i, j and k integers gives rise to orbitals of different shells (s,p,d) [60]. To solve the problem that a STO is impractical and GTOs are not precise it is possible to make up an STO from many GTOs [66]. A set of GTOs that is made to imitate a STO is called a *contracted* Gaussian. If more Gaussian orbitals are included, the Slater type orbitals are more accurately reconstructed, and the computation becomes more precise.

Since each basis function is a one-electron wavefunction, the minimum basis set of an atom has the same size as the number of orbitals. For example the minimum basis set of carbon has 5 basis functions since the accessible electronic orbitals are: $1s$, $2s$, $2p_x$, $2p_y$ and $2p_z$. In this minimal case each orbital is represented by a single basis function. If one wants to increase the computational accuracy, more electron locations must be allowed per orbital. This is done by adding more basis functions with slightly different sizes than the minimal one. For example a more advanced basis set for carbon would be: $1s$; $1s'$, $2s$; $2s'$, $2p_x$; $2p'_x$, $2p_y$; $2p_y$'and $2p_z$; $2p'_z$ where the primed functions differ slightly in position to the non-primed ones. The 'true' wavefunctions are then expressed as linear combinations of the basis functions. Another method is to add basis functions with higher angular momenta to the basis set [66]. In the case of carbon these would be the d, f and higher functions.

A perfect (complete) basis set contains an infinite amount of basis functions and would leave the electrons in the system completely unrestrained. Of course this would take too large a toll on our computation power. Therefore it is important to identify which orbitals matter the most in the system under investigation and choose the basis set accordingly. There are many specialized basis sets on the market that cater to specific needs, for example, heavy atoms, or highly charged ones [66]. The choice of basis set matters less as its size approaches the complete basis since the electron wavefunctions become more and more unconstrained. This leads to the general rule of thumb that 'bigger is better'. In any case, one should compare several basis sets to find the one that yields the most precise results.

5 Calculations and enhancement factors

After the general outline of the research given in chapter 3 and the computational theory of chapter 4 it is now time to put this knowledge into practice. We need to determine two things: to identity promising, quasi-degenerate rovibrational transitions and to determine the enhancement factors of these transitions.

To this end I will start with a detailed overview of the molecules of which the enhancement factors were calculated. After this there will be section on the theory of calculating numerical values for the enhancement factors. Then I will discuss how the computational techniques highlighted in chapter 4 have been used to accomplish the two goals. Finally the obtained results will be presented separately for each group of molecules.

5.1 Molecule overview

The entire set of systems consists of the following diatomic molecules: Ge_2^+; Sn_2^+; As_2^+; Sb_2^+ $SiSe^+$; $SiTe^+$; SeO^+; TeO^+; C_2^+; O_2^+; Cl_2^+; S_2^+; SO^+ and PbS^+. These molecules were selected by comparing the energies between the low-lying electronic levels with the size of the harmonic

constant ω_e. If the energy gap is more or less a multiple of ω_e then quasi-degenerate levels are expected be present. This makes this set of molecules of particular interest for future research into the variation of the fundamental constants.

What these molecules also have in common is that they are all singly charged positive ions. The benefit of using ions is that they are more easily trapped and manipulated by electric fields in experiment. This underlines the importance of performing calculations that are relevant not only for theorists but also for experimentalists.

The electron configuration of the molecules is similar, with all of them (except C_2^+) having a $^2\Pi$ ground state. This similarity makes it easier to set up the calculations. Additionally the dependence of a doublet $^2\Pi$ state on the fine structure constant α is known analytically, which is useful if this fine structure transitions are probed specifically.

The molecule set is split in two groups. A different computational technique will be employed for both of these groups. The goal of determining the enhancement factors is still the same for both subgroups, however. The specifics for each group are given below.

Table 1: Spectroscopic constants of the $X^2\Pi$ state of the first group of molecules. Empty columns are included to indicate for which constants there is no data available. R_e is the bond length, B_e the rotational constant, D_e the centrifugal distortion constant, ω_e the harmonic constant with $\omega_e x_e$ as a first correction and A_e is the fine structure splitting.

	R_e (Å)	$B_e(cm^{-1})$	$D_e(cm^{-1})$	$\omega_e(cm^{-1})$	$\omega_e x_e(cm^{-1})$	$A_e(cm^{-1})$	reference and method
Ge_2^+	2.410[a] 2.475[a] 2.407[b]			258.6[a] 256[a] 209[b]	1.94[b]		a, [67], DFT* b, [68], CI**
Sn_2^+	2.776[a] 3.045[b] 3.060[c]			173.9[a] 143[b] 143[c]	.32[b] .32[c]		a, [67], DFT b, [68], CI c, [69], CI
$SiSe^+$	2.22[d]			455[d]			d, [70], CI
$SiTe^+$	2.45[e]			384[e]			e, [71], CI
PbS^+	2.56[f]			363[f]			f, [72], CI
SeO^+	1.597[g]			1035.5[g] 999.7[h]	9.62[g] 6.31[h]		g, [73], CC*** h, [74], **experiment**
TeO^+						4840[h]	h, [74], **experiment**
As_2^+	2.230[i] 2.230[i]			385[i] 347[i]			i, [75], **experiment** i, [75] CASSCF****
Sb_2^+	2.66[i]			227[i]			i, [75], CASSCF

*DFT: density functional theory
**CI: configuration interaction
***CC: coupled cluster
****CASSCF: complete active space, self consistent field

5.1.1 Molecule group I: Ge_2^+; Sn_2^+; As_2^+; Sb_2^+ $SiSe^+$; $SiTe^+$; SeO^+, TeO^+ and PbS^+

For the first group only fine structure transitions were investigated. Fine structure transitions are particularly nice to investigate because their very existence is due to α. Not only does this mean that the dependence of these transitions on α is known analytically, it also ensures that the energy levels behave differently under α variation. If the levels depend similarly on α their net change under α variation would be less, lowering the enhancement factor.

In order to find the quantum numbers of sensitive quasi-degenerate levels the potential energy curves of the two fine structure levels have to be known. To determine these energy curves, and also to quantize the inherent sensitivity we need precise values for the spectroscopic constants. The spectroscopic constants are known experimentally only for As_2^+ and Sb_2^+ and even for those molecules there is not enough information to accurately reproduce the curves. For the other molecules only calculated values for the spectroscopic constants are known, but with too low precision to be used for this research. An overview of the constants obtained from other sources can be found in Table 1.

The lack of reliable data meant that the spectroscopic constants had to be calculated for this molecule group. This was done using the SRCC and MRCC methods. Tables of the constants I calculated are located in appendix B (Tables 8 - 11).

5.1.2 Molecule group II: C_2^+, O_2^+, Cl_2^+, S_2^+ and SO^+

For the second group of molecules transitions between electronic states were probed. This means that the analytic expression for the enhancement factor K_α can not be used for this group of molecules so that another approach had to be taken. Luckily, the spectroscopic constants of the first few energy levels of this group of molecules are already known from experiment, which saves us the trouble of having to use high precision calculations to determine the potential energy curves. It also allows us to determine the promising, quasi-degenerate levels from the experimental constants. Additionally, since spectroscopic experiments have already been performed for this set of molecules the chance of them being suited for research into the variation of fundamental constants goes up. The values of the spectroscopic constants as obtained from experiment can be found in appendix F (tables 16 - 20), as well as a selection of rotational transitions. The potential energy curves and the resulting vibrational and rotational levels were kindly provided by Lukáš Pašteka of the Comenius University [76].

5.2 α and μ dependence of a transition energy

The goal of this research is to quantify the sensitivity to the variation of the fundamental constants of the transitions in our molecule set. This allows us to compare the molecules to each other and provide a sensitive system to be used in experiment. The quantification comes in the form of the enhancement factors of a transition, where a higher factor means a more sensitive transition.

To determine the enhancement factors of a transition we need to know the dependence of the transition energy on the fundamental constants. The transition energy does not depend directly on the fundamental constants, but rather on the spectroscopic constants. The necessary spectroscopic constants are: the harmonic frequency ω_e, the rotational constant B_e, the centrifugal distortion constant D_e and the transition energy T_e. In the case of a fine structure transition T_e is the vibrotationally dependent spin-orbit coupling constant A_e.

We start by writing down the relative change in the transition frequency ω as function of μ and α:

$$\frac{\delta\omega}{\omega} = \frac{\delta\omega}{\delta\mu}\delta\mu\omega^{-1} + \frac{\delta\omega}{\delta\alpha}\delta\alpha\omega^{-1} \tag{27}$$

To show equation 27 more explicitly we can write the frequency of a transition from the (vibration, rotation) = (ν_2, J_2) level to the (ν_1, J_1) level expressed in terms of the spectroscopic constants in the following way:

$$\begin{aligned}\omega = \frac{\Delta E}{hc} =& -\omega_e(\nu_2-\nu_1) + \omega_e x_e(\nu_2-\nu_1)(\nu_1+\nu_2+1) + h.o \\ & - B_e(J_2-J_1)(J_1+J_2+1) + h.o. + T_e.\end{aligned} \tag{28}$$

Which is nothing but the basic energy difference of two vibrational states corrected with anharmonicities and rotations. The higher orders are usually neglected since each of them is an order of magnitude smaller then the last.

The dependences of the spectroscopic constants on μ are known. In the approximation of a perfect harmonic oscillator the frequency scales as $m^{-1/2}$ where m is the mass of pendulum. In the case of diatomic molecules the pendulum mass is the reduced mass of the molecule, which is directly related to the proton-to-electron mass ratio and thus $\omega_e \sim \mu^{-1/2}$. The first anharmonicity $\omega_e x_e$ scales as ω_e^2 and thus $\omega_e x_e$ is proportional to μ as $\sim \mu^{-1}$. In the linear rotor approximation the rotational energy splitting B_e scales as μ_m^{-1}, where μ_m is the reduced mass of the molecule [60]. Again the relation between the reduced mass and the proton-to-electron mass ratio is linear so that $B_e \sim \mu^{-1}$. any α dependence of the spectroscopic constants is neglected, as well as the dependence of the transition energy T_e on μ [77].

By combining equation 27 and 28 and writing it in the form of equation 29 we may identify the enhancement factors as a function of the spectroscopic constants:

$$\frac{\delta\omega}{\omega} = K_\mu\frac{\delta\mu}{\mu} + K_\alpha\frac{\delta\alpha}{\alpha} \tag{29}$$

With the enhancement factors:

$$\begin{aligned}K_\mu =& \big[\frac{1}{2}\omega_e(\nu_2-\nu_1) - \omega_e x_e(\nu_2-\nu_1)(\nu_1+\nu_2+1) \\ & + B_e(J_2-J_1)(J_1+J_2+1)\big]\omega^{-1} \\ K_\alpha =& \frac{\delta T_e}{\delta\alpha}\alpha_0\omega^{-1}\end{aligned} \tag{30}$$

High values for K_μ and K_α in equation 29 indicate a larger change in the transition frequency ω, even if the change in the fundamental constants $\delta\alpha$ and $\delta\mu$ is small. The fact that the enhancement factors are inversely proportional to ω enforces the importance of quasi-degenerate transitions to maximize the sensitivity to the variation of the fundamental constants.

The enhancement factors of equation 30 are relative to the transition they belong to, as indicated by their dependence on ω. We search for transitions with small ω values. Therefore small calculational errors might affect the results significantly. Thus it may be useful to look at the absolute enhancement factors $\bar{K}_\mu$ and $\bar{K}_\alpha$. They are related to the relative enhancement factors as:

$$\begin{aligned}\bar{K}_\mu =& K_\mu\omega = \frac{1}{2}\omega_e(\nu_2-\nu_1) - \omega_e x_e(\nu_2-\nu_1)(\nu_1+\nu_2+1) \\ & + B_e(J_2-J_1)(J_1+J_2+1) \\ \bar{K}_\alpha =& K_\alpha\omega = \frac{\delta T_e}{\delta\alpha}\alpha_0\end{aligned} \tag{31}$$

Although the absolute enhancement factors are an indication of the inherent sensitivity of a molecule to the variation of fundamental constants they still depend on the energy level quantum numbers. The values are, however, much more robust against calculational errors.

Without knowing the dependence of T_e on α equation 30 is not very helpful. In general $T_e(\alpha)$ is not known except for fine structure transitions. So for the first group of molecules, for which only fine structure transitions are probed, we have:

$$T_e = A_e \sim Z^2\alpha^2 \sim \alpha^2 \tag{32}$$

so that K_α reduces to:

$$K_\alpha = 2A_e\omega^{-1} \tag{33}$$

In the cases for which the dependence of T_e on α is not known analytically it is possible to determine the dependence empirically by calculating T_e for various α. In the linear regime the slope of the resulting curve then gives $\frac{\delta T_e}{\delta \alpha}$. Unlike in a real experiment, in a calculational setting we are not limited by our inability to vary the fine structure constant. This makes it possible to simulate the experiment described above and obtain the K_α enhancement factor up to calculational precision.

In a recent study many diatomic molecules were investigated [45] and relative enhancement factors up to $\sim 10^6$ for α and $\sim 10^5$ for μ have been found. The hope is to find enhancement factors comparable to this level in the current sample. Even if that is not the case, it should be noted that enhancement factors are not everything. Ultimately the molecules will have to be cooled and trapped, for which other properties than just a high enhancement factor may be decisive. Therefore it is always useful to add more molecules to the pool of molecules that would be favorable for experimental research.

5.3 Computational details

Although the influence of the choice of Hamiltonian, basis set and computational method was discussed in chapter 4, little information has been provided on the methods I chose to use for this specific case. This information will be provided in the following section.

The biggest difference between the two groups of molecules is the computational method that was used. For the first I used the relativistic coupled cluster method and for the second I used the configuration interaction method. As mentioned in chapter 4, one would prefer to use the CC method since it is more precise and less computationally expensive. Using this method was only possible for the first group of molecules, for which just the ground state and the first excited state had to be calculated. For the second group, for which the ground state and the first few excited states had to be calculated, the CC method is unsuited as it can only handle states that differ slightly from the ground state (S_2^+ is an exception for which CC was still viable). Since both methods are included in the DIRAC15 package, switching between the two was not a large problem.

As far as the procedure for the two molecule groups was the same the two are discussed together. This is mostly the case for the Hamiltonian that we needed to include relativity in both cases and the basis sets. Afterwards, the important computational parameters will be discussed for each group individually.

5.3.1 Hamiltonian and basis sets

A X2C Hamiltonian that is included in the DIRAC15 package was used for the entire molecule set [78]. This was done in an effort to save computer resources as much as possible. The error introduced by using this Hamiltonian should be small since the X2C Hamiltonian was shown

to accurately reproduce transition energies. As extra confirmation I ran a calculation on PbS^+ again with both the X2C and a 4-component Hamiltonian. Since PbS^+ is one of the heaviest molecules in the set the error induced by the use of the X2C Hamiltonian should be the largest for this system. The energies of the calculations differed only by $12cm^{-1}$ on a total energy of $21300cm^{-1}$ of the fine structure transition. If the error in such a heavy molecule is this small the use of the X2C Hamiltonian is certainly justified.

The choice of basis set for the molecules is slightly more complex than choosing a Hamiltonian. As mentioned in chapter 4, we wish to use a basis set that is as large as possible without straining the computational resources too much. To achieve this I ran a few calculations for each molecule using different basis sets. These trial basis sets included: cc-pVTZ [79], cc-pVQZ [79], dyall.v4z [80] and augmented versions of these preloaded sets. A basis set can be augmented by increasing its size by manually adding diffuse (i.e. low exponent) orbitals to the set.

The property of interest is the transition energy and not the total energy of the system. Thus rather than using a basis set that gives precise electronic energies, we look for a set that gives precise transition energies. By using the trial calculations the most optimal basis set was determined for all molecules. The process of finding an optimal basis set is called reaching *convergence with respect to the basis set*. If a calculation is converged with respect to the basis set the computational cost of adding more basis functions is not worth the increase in precision. In the case of the first set of molecules convergence was reached usually at the doubly augmented level (d-aug-cc-pVQZ, d-aug-dyall.v4z). There were however also some cases in which a larger or smaller set was needed. An overview of which basis set was used for each molecule can be found in Table 3 and 4 for the first and second molecule group respectively.

5.3.2 Spectroscopic constants and correcting the FSCC curves of the first molecule group

For the first group of molecules, the first goal is to retrieve the spectroscopic constants from the potential energy curves. After the computations have converged with respect to the basis set it is quite easy to run the program for several (6-8) bond lengths. The graph of these energies as a function of the bond length then gives the potential energy curve. A separate program called Dunham, written by V. Kellö of the Comenius University [81] was used to calculate the spectroscopic constants. It is based on the work of, and named after, J. Dunham [82, 83]. We would like to use the results of the FSCC module as input for the Dunham program, since it is well suited to calculating transition energies. However, the SRCCSD(T) module is more precise as it includes a higher order of electron correlation.

The extra correlation in the SRCCSD(T) module comes from the perturbative inclusion of triple electron excitations. By running both a SRCCSD and a SRCCSD(T) calculation, the contribution of triple excitations can be extracted. It is then possible to add this difference to the FSCC calculations manually. Since the addition was perturbative it stands to reason that the results would be similar if this feature was included in the FSCC module. The resulting 'corrected FSCC' curves were then used to obtain the final spectroscopic constants and enhancement factors.

The difference in the shape of the potential energy curve obtained from the SRCC and FSCC methods should not be too large, i.e. the spectroscopic constants should be similar. To check this, spectroscopic constants have been obtained for all curves for comparison. This comes down to 4 sets of spectroscopic constants per molecule.

After running the computations, fixing the bugs, and rerunning them until they work it is possible to extract the spectroscopic constants. This almost allows us to solve equation 30, except for the specific quantum numbers of the transition. In order to find those, the spectroscopic constants are inserted into a Mathematica program written by Lukáš Pašteka [76]. This program

converts the spectroscopic constants back into a potential energy curve and also adds vibrational levels. Quasi-degenerate levels can then easily be found by eye. All potential energy curves found in this work are made using this Mathematica program. A different part of the program allows us to zoom in on a particular vibrational level and adds the rotational energies to it. This allows us to reduce the transition energy even further. After the rotational and vibrational quantum numbers have been obtained in this way the enhancement factors can be calculated.

5.3.3 The CI method and finding $\frac{\delta T_e}{\delta \alpha}$ for the second molecule group

For the second molecule group we already know the spectroscopic constants and the favorable transitions. So the only goal is to obtain the enhancement factors themselves. Instead of looking only at fine structure transitions, as is the case for the first molecule group, I also investigated electronic transitions. This means that equation 33 can not be used to calculate the enhancement factor K_α for these molecules as the dependence of a general electronic transition on α is not known analytically. Instead equation 30, and in particular the $\frac{\delta T_e}{\delta \alpha}$ term must be solved directly. This is done by calculating T_e for several values of α and determining the slope of the resulting curve. This is valid as long as the $T_e(\alpha)$ can be approximated by a straight line, which is the case for these calculations.

Within the DIRAC15 package there is no way to directly alter the value of the fine structure constant α. There is, however, an option to vary the speed of light. In atomic units $\alpha = \frac{1}{c}$ and c is approximately 137. This makes it straightforward to vary α in the calculations. I chose to vary the value of c (α) by 10% from the current value in intervals of 5%. This corresponds to an input of: 123.4, 130.2, 137, 143.8 and 150.7. Where 137 is the current value of the speed of light (and thus of α). In this case the dependence of T_e to α proved to be linear. Higher values of c indicate relativistic effects are less (smaller α) and lower values indicate the opposite (larger α). In a real experiment the shift in α would be a fraction of a fraction of a percent, incomparable to the ten percent that is used in the calculations. I stress however, that the important information comes from the slope of the transition energy as function of α rather than the absolute energies of the levels.

When calculating the electronic transition energies it is important to take into account that the average bond length R_e changes much more dramatically between different electronic states than it does for fine structure states. We wish to obtain adiabatic transition energies, i.e. transitions for which the states are at their optimal bond lengths. It is for this reason that the calculations for each c value were run at several bond lengths (usually 5, unless no minimum was found) around the suspected minima of the potential energy curve of each electronic state. Using fewer points reduces the accuracy of the resulting potential energy curve, but still gives an accurate average bond length. The precise shape of the energy curve is relevant only for obtaining the spectroscopic constants, which are already known. After a reasonably precise minimum is obtained in this fashion an additional calculation can be run to obtain the actual energy difference between the states in question.

In the CI procedure electron correlation is included by expanding the reference wavefunction with configuration wavefunctions. These configurations have to be added by defining a Generalized Active Space (GAS) [84]. All configurations between electrons in this GAS are included in the CI procedure. Being new to this method, I tried to use as large a GAS as possible to include many configurations. An overview of the GAS spaces of the molecules is given in appendix A, table 7. It is possible that I accidentally excluded important configurations. This will be addressed in more detail when the validity of the CI calculations is discussed.

5.4 First group results

Not every molecule in the first set yielded usable results. In the case of Sb_2^+, SeO^+, $SiSe^+$, TeO^+ and $SiTe^+$ there were computational problems. These problems are mostly due to the $X^2\Pi$ state being crossed by a close-lying Σ state. The interaction with this third state heavily influences the shape of the potential energy curves, which makes the external programs necessary to obtain the spectroscopic constants unusable. The potential energy curves of the doublet $^2\Pi$ state of $SiSe^+$ and SeO^+ including the crossing Σ states have been determined. Further analysis may still identify the vibrational and rotational levels needed to determine their enhancement factors. These five molecules will not be discussed further in this work.

5.4.1 Validity of spectroscopic constants

Tables with the calculated spectroscopic constants for each molecule can be found in appendix B (Tables 8 - 11). The mass that was used as input for the Dunham program with which these constants were calculated can also be found in these tables. An overview of the previous values can be found in Table 1. For completeness and easy comparison these values are repeated in the tables of the constants of their respective molecule. In general the difference between

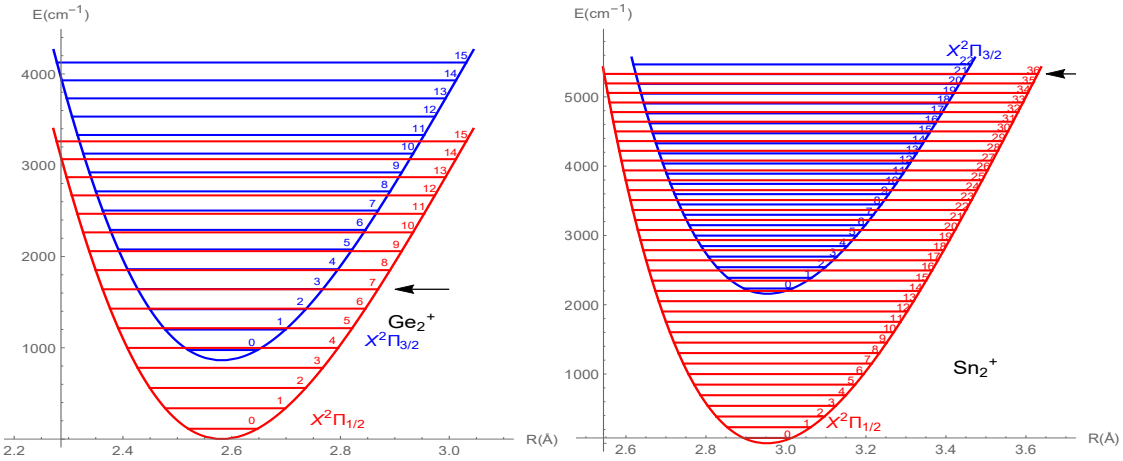

Figure 5: Potential energy curves of the substates of the $X^2\Pi$ state of Ge_2^+ and Sn_2^+. Horizontal lines indicate the quantized vibrational levels, with arrows pointing to levels of quasi-degeneracies. These quasi-degenerate levels are 3-7 for Ge_2^+ and 21-36 for Sn_2^+.

earlier results and my calculations is on the order of a few percent. This difference is to be expected considering the different computational methods used and the different basis sets that are employed. The most accurate constants will always come from experiment and those are only available for As_2^+, Sb_2^+ and SeO^+. Of these three molecules only As_2^+ yielded calculational results to compare to experiment. The precision of the calculations for As_2^+ is very high, which makes the other results all the more credible.

Another way to check the validity of the calculated constants is to compare the FSCC, CCSD and CCSD(T) results with each other. Again the values differ only slightly. This means that the shape of the potential energy curve is consistent over multiple calculational methods and should thus be close to its real shape.

The most precise method employed in previous work is the CI method. This method is good, but is less precise then the CC method for the same basis set. Considering the small discrepancy

between the used methods and the similarity between the As_2^+ result and experiment I conclude that my constants can be trusted to be close to their real values. Since the method I employed is considered to be the most suited for this purpose I will even claim that the spectroscopic constants I calculated are the most precise to date.

5.4.2 Potential energy curves

The potential energy curves obtained for each molecule are included in appendix C (Figure 9 - 10), with those of Ge_2^+ and Sn_2^+ added in Figure 5 as an example. These potential energy curves have all been drawn with the Mathematica program. We used only the spectroscopic constants calculated using the corrected FSCC method as input. Vibrational levels have been included in these curves and arrows indicate which pairs of vibrational levels are quasi-degenerate. The transition energy between the two states indicated by the arrows is on the order of a few cm^{-1}. All curves are consistent with what one would expect from fine structure splitting, including the similar shape of the two states and the size of the fine structure splitting. The crossing of the levels for PbS^+ is consistent with the shape of the curves found in earlier work [72].

5.4.3 Rotational levels and enhancement factors

Although the splitting between two close-lying vibrational levels is on the order of a few cm^{-1} the difference is still too large to yield significant enhancement factors. Therefore we add rotational levels to the vibrational ones that were already determined to be quasi-degenerate (indicated by the arrows). The resulting rotational transitions are included in appendix D (Figure 11 - 12). Again the rotational levels of Ge_2^+ and Sn_2^+ have been added as an example, see Figure 6. In each case the smallest transition and the two neighboring transitions have been indicated. The final transitions are on the order of a few hundreds of cm^{-1} up to a few tenths of cm^{-1}.

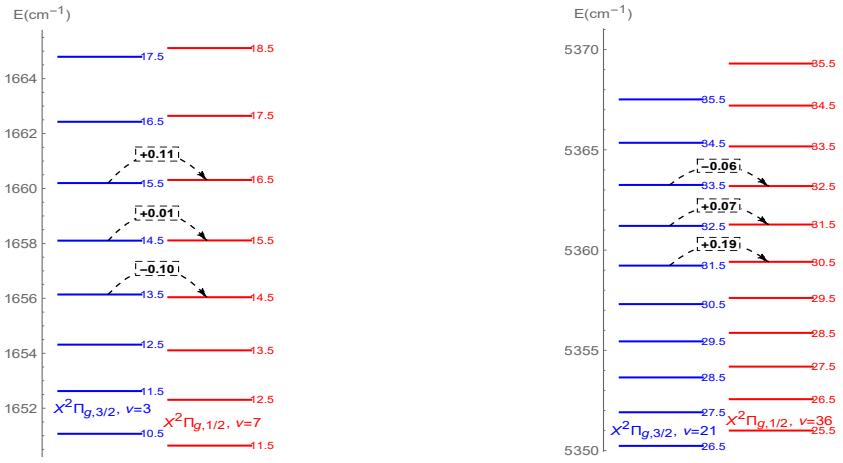

Figure 6: Rotational energy levels of Ge_2^+ and Sn_2^+ as imposed on their indicated vibrational levels. Quasi-degenerate transitions and their energies are indicated by arrows.

Due to a coupling between the electron spin and the molecular vibration an additional splitting takes place. This phenomenon is known as Λ-doubling and manifests itself as a splitting of the rotational levels. The strength of this doubling in the pure precession approximation is given by [85, 86]:

$$\Delta E(^2\Pi_{1/2}) = \frac{4B_e(A_e+2B_e)}{\Delta E_{\Sigma\Pi}}(J+\tfrac{1}{2}) \tag{34}$$

$$\Delta E(^2\Pi_{3/2}) = \frac{12B_e^3}{A_e\Delta E_{\Sigma\Pi}}(J+\tfrac{1}{2})(J-\tfrac{1}{2})(J+\tfrac{3}{2}) \tag{35}$$

In which $\Delta E_{\Sigma\Pi}$ is the transition energy to the first Σ state above the doublet $^2\Pi$ ground state. Equations 34 and 35 were evaluated by performing an additional FSCC calculation to determine $\Delta E_{\Sigma\Pi}$. The results of this calculation can be found in Table 2. For all four molecules the size of the Λ doubling of the $^2\Pi_{1/2}$ state was found to be on the order of 10^{-1} cm^{-1} per rotational quantum number. The lambda doubling for the $^2\Pi_{3/2}$ state is at least five orders of magnitude smaller than that. In comparison to the error in the calculations the effect of Λ doubling is extremely small for these molecules and will be neglected. Once the quantum numbers of the selected quasi-degenerate levels are known, equation 30 can be evaluated. The resulting enhancement factors are shown in Table 3. Both the absolute and relative enhancement factors are shown, as well as the used basis set. Only the highest enhancement factors are shown for each molecule. More detailed tables with enhancement factors calculated in several ways can be found in appendix E (Table 12 - 15). In comparison to results obtained in [45] the enhancement factors obtained in this work are slightly above average. This means that the four included molecules are certainly worth considering when setting up a new experiment into the variation of the fundamental constants.

Table 2: Transition energy between the $X\Pi$ and $A\Sigma$ states used to calculate Λ-doubling.

Molecule	$\Delta E_{\Sigma\Pi}$ cm^{-1}
Ge_2^+	3451
Sn_2^+	3512
As_2^+	3125
PbS_2^+	6342

Table 3: Enhancement factors from corrected FSCC calculations. Transition quantum numbers are given as (vibrational, rotational). The addition '+hh' of a basis set indicates that two h-type functions have been added to the set manually.

	K_μ	K_α	$\bar{K}_\mu$ (cm^{-1})	$\bar{K}_\alpha$ (cm^{-1})	Transition	Basis set
Ge_2^+	-40931.9	-172458.5	-409.3	-1724.6	$(7, 14.5) \rightarrow (3, 15.5)$	d-aug-cc-pVQZ+hh
Sn_2^+	-16396.1	-71904.1	-983.8	-4314.2	$(36, 32.5) \rightarrow (21, 31.5)$	d-aug-cc-pVQZ+h
As_2^+	29643.8	-137982.9	592.9	-2759.7	$(28, 6.5) \rightarrow (32, 5.5)$	aug-cc-pVQZ
PbS^+	10680.7	-159487.4	106.8	-1594.4	$(25, 11.5) \rightarrow (27, 12.5)$	d-aug-dyall.v4z

5.5 Second group results

Since the spectroscopic constants of the molecules of the second group are already known from experiment the calculations for this group will discussed later in this section. First I will go over the favorable transitions that were determined from the spectroscopic constants. After this the dependence of these favorable transitions on variation on α will be determined by calculating the transition energies for several α and the resulting enhancement factors will be presented.

5.5.1 Favorable transitions

The potential energy curves from which the favorable rovibrational transitions were determined were made using the same Mathematica program that was used for the first molecule group. The only difference is that the spectroscopic constants that are used as the input of this program were obtained from experiment rather than calculation. The experimental spectroscopic constants that were used to produce the curves is included in appendix E (Table 17 - 20). These curves were produced by Lukáš Pašteka of the Comenius University. An example of one of the curves has been included in Figure 7.

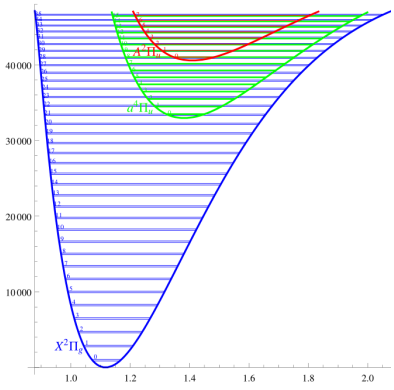

Figure 7: Potential energy curves of the first few electronic states of O_2^+. Courtesy of Lukáš Pašteka [76].

Vibrational levels were included in the potential energy curves in the same way as was done for the first group. On top of the most close-lying vibrational levels the rotational levels could then be plotted. There are many more transitions between quasi-degenerate levels since there are more states. The plot of the rotational levels containing the most optimal transition of each molecule can also be found in appendix F (Figure 13 - 15).

In addition to having a transition between quasi-degenerate states the intrinsic sensitivity to the variation of the fundamental constants of a molecule must be high for it to be suitable for research. The intrinsic sensitivity to μ variation is dependent on the spectroscopic constants and can be determined from equation 30 without problems. The sensitivity to α had to be calculated since its analytic value is only known for fine structure transitions. The results of these calculations can be found in the next sections.

5.5.2 Validity of energy differences

For the second molecule group we are less interested in the shape of the potential energy curve since it is already known from experiment. The first goal is to precisely determine the adiabatic transition energy T_e between each of the electronic states. This means that we need to calculate the energy difference between the states as they are at their optimal bond length. Several calculations were run for each state to determine this optimal bond length and little error is expected in their values.

By comparing the transition energies to experiment we can validate the calculations rigorously. A comparison between the calculated and measured transition energies is given in Table 4. It is important to note that the calculations give all substates of an electronic state, whereas often only the average state was investigated in experiment. To be able to compare the calculations to experiment the calculated energies of the substates were averaged.

In most cases the calculational precision is very high, with differences to experiment being at most a few percent and often much less then a percent. The Cl_2^+ molecule is the exception

Table 4: Electronic excitation energies from the ground state in cm^{-1}. Compared with experimental results of the same transitions. The energy of the states is obtained by averaging the energies of the states that comprise it.

	Calculation	Experiment	Difference (%)	Basis set
$\mathbf{C_2^+}$				d-aug-cc-pVQZ
$X^4\Sigma_g^-$	0	0	0	
$B^4\Sigma$	19778.0	19652.2	0.64	
$\mathbf{SO^+}$				aug-cc-pVQZ
$X^2\Pi$	0	0	0	
$A^2\Pi$	31738.20	31421.49	1.0	
$a^4\Pi$	23934	25474	6.0	
$\mathbf{O_2^+}$				aug-cc-pVQZ
$X^2\Pi$	0	0	0	
$A^2\Pi$	40550.276	40572.785	0.06	
$a^4\Pi$	31648.8	32962.2	4.0	
$\mathbf{S_2^+}$				d-aug-dyall.v4z
$X^2\Pi_g$	0	0	0	
$A^2\Pi_u$	22209.55	22354.45	0.65	
$\mathbf{Cl_2^+}$				d-aug-cc-pVQZ
$X^2\Pi_{g,3/2}$	0	0	0	
$a^4\Sigma^-_{u,1/2}$	15322.4	17114.1	11.5	
$a^4\Sigma^-_{u,3/2}$	15365.0	17151.6	11.4	
$A^2\Pi_{u,3/2}$	18469.50	20440.81	9.8	
$B^2\Delta_{u,3/2}$	20664.31	21913.42	5.7	

to the rule, with the calculated energies being much less then expected. There could be many explanations for this, including some unexpected behavior of the orbitals that is not included in DIRAC15. More likely however, is an error in the configuration space included in the evaluation of the orbitals as was discussed in section 5.3.3. Although the absolute values of the Cl_2^+ transitions is far of from the experimental values, the obtained enhancement factors for this molecule are still reasonably precise. This is because they are obtained from the change in these energies, rather than their absolute values. Nonetheless, the inaccuracy will be investigated further.

5.5.3 Curves and enhancement factors

When the calculated electronic states have been identified with those from experiment it is straightforward to run the calculations for several values of c. The result of those calculations is a range of transition energies at different speeds of light. By plotting these energies as function of $\alpha = \frac{1}{c}$ the slope of the curve can be obtained. An example of such a curve is given in Figure 8.

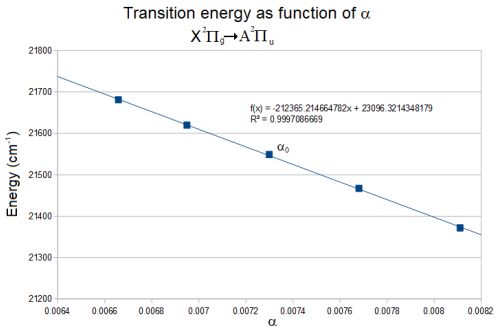

Figure 8: Fit to the transition energy of the $X^2\pi_g \rightarrow A^2\Pi_u$ transition in S_2^+ calculated at different values of α. The equation of the fit as well as its R^2 value have been included.

The slope of the curve is then equal to $\frac{\delta T_e}{\delta \alpha}$, with which equation 30 can be evaluated. This has been done for every transition between the low lying levels of the molecules in the second set. The resulting absolute enhancement factors can be found in appendix G (Table 21 - 25). Note that the tables are antisymmetric. Going form one state to another or the other way around flips the sign of the enhancement factor but does not change its magnitude. This means that it is always more useful to look at the absolute values of the factors displayed in the tables when comparing the sensitivities to each other. The values range from ∼10 for a transition in SO^+ to ∼1500 for transitions in Cl_2^+.

These values are lower than the values found in the first set of molecules. The difference being an order 2 to 3. The smaller absolute enhancement can be overcome by probing the quasi-degenerate levels that were determined earlier (appendix F). The relative enhancement factors belonging to the close-lying levels are provided in appendix H (Table 26 - 28). Not every transition had an accompanying quasi-degeneracy, as indicated by the "no q-d" label in the tables. For the C_2^+ and S_2^+ molecules no quasi-degenerate rovibrational transitions could be identified altogether, so only the absolute K_α enhancement factor could be determined. Their values are not reported here, but have been included in appendix G.

An overview of the most promising transitions has been included in Tables 5 for K_α and 6 for K_μ. Enhancement factors for α were determined for every electronic transition in the molecules, but only the most promising ones are shown in Table 5. The K_μ factors were calculated only for these promising transitions. The highest relative α enhancement of this group is found in a transition of Cl_2^+. Of special note are the high absolute μ enhancement factors of O_2^+ and SO^+. If even more narrow transitions can be identified for these molecules they may prove to be good candidates for future research.

Table 5: K_α enhancement factors, CI calculations.

	$\bar{K}_\alpha$	K_α	transition	quantum numbers (ν, J)
Cl_2^+	-1038	-20760	$X^2\Pi_{g,3/2} \rightarrow A^4\Sigma_{u,1/2}$	(42, 9.5) → (19, 8.5)
	-1460	-14600	$X^2\Pi_{g,3/2} \rightarrow A^2\Pi_{u,3/2}$	(42, 8.5) → (6, 9.5)
O_2^+	-362	905	$X^2\Pi_{g,3/2} \rightarrow a^4\Pi_{u,3/2}$	(28, 17.5) → (8, 18.5)
SO^+	-578	5780	$X^2\Pi_{3/2} \rightarrow a^4\Pi_{3/2}$	(25, 26.5) → (3, 27.5)
	455	4550	$X^2\Pi_{1/2} \rightarrow a^4\Pi_{-1/2}$	(32, 13.5) → (10, 14.5)

Table 6: K_μ enhancement factors

	$\bar{K}_\mu$	K_μ	transition	quantum numbers (ν, J)
Cl_2^+	5508.9	110178	$X^2\Pi_{g,3/2} \rightarrow A^4\Sigma_{u,1/2}$	(42, 9.5) → (19, 8.5)
	-6904.2	-69042	$X^2\Pi_{g,3/2} \rightarrow A^2\Pi_{u,3/2}$	(42, 8.5) → (6, 9.5)
O_2^+	-10109.3	25273	$X^2\Pi_{g,3/2} \rightarrow a^4\Pi_{u,3/2}$	(28, 17.5) → (8, 18.5)
SO^+	-10276	102759	$X^2\Pi_{3/2} \rightarrow a^4\Pi_{3/2}$	(25, 26.5) → (3, 27.5)
	-10117.9	101179	$X^2\Pi_{1/2} \rightarrow a^4\Pi_{-1/2}$	(32, 13.5) → (10, 14.5)

6 Conclusions and discussion

Between the two methods, relative α enhancement factors on the order of 10^5 have been obtained for Ge_2^+, As_2^+ and PbS^+. The relative μ enhancement factors were on the same order of magnitude in Cl_2^+ and SO^+.

A better way of interpreting the results may be to look at the absolute, rather than the relative enhancement factors. The absolute enhancement factors are more heavily dependent on the inherent molecular properties than the quasi-degeneracy of the energy levels. Since the qausi-degenerate levels are hard to identify precisely using calculation absolute enhancement should be weighed higher than relative enhancement. The molecules with the highest absolute enhancement factors are Sn_2^+ and O_2^+ for α and μ respectively. Sn_2^+ has an absolute α enhancement of -4$\times$ 10^3 cm^{-1} and O_2^+ has a μ enhancement of -10^5 cm^{-1}.

To obtain the enhancement factors of the first molecule group their spectroscopic constants were calculated with high precision. The values of these constants presented in this work are the most precise values of these constants to date.

As mentioned before, transitions with relative α enhancement factors up to 3×10^6 have been identified in an I_2^+ transition [45]. This factor is an order of magnitude higher than the values reported in this work. Many other molecules were investigated in the same work, with most having α enhancement factors on the order of 10^4. This ranks the molecules investigated in this work as above average, but not as the most sensitive.

It should be noted that it is hard to make a definitive ranking of molecules that should be used in experiment. When setting up an experiment more factors than just the enhancement factors play a role. The ease of trapping and cooling might be much more important for example. This is why finding more sensitive molecules is always worth the effort, even if their enhancement factors are not the highest. Of the molecules investigated in this work, Cl_2^+, O_2^+, Ge_2^+ and As_2^+ are particularly sensitive and should be considered when a new experiment is being set up.

There are caveats that should be added to the results above. Although the calculations are of high quality and large basis sets were used the fact that exact results can not be obtained still remains. This means that one should expect an error in the rovibrational energy levels on the order of $\sim$10 cm^{-1} and potentially more. Considering that the enhancement factors are based on transitions that are only tenths of inverse centimeters large, this error might change the favorable transitions completely. This is why by no means I claim to provide the exact transitions that should be probed. I do, however, claim that there is likely to be a favorable transition present in the neighborhood of the identified transitions. This point is less relevant for the absolute enhancement factors, which are not amplified by the quasi-degeneracy of certain states. Even the absolute enhancement factors depend on the quantum numbers of the transition, however,

and are thus affected by the calculational errors.

Another point of concern is the fact that some of the vibrational levels calculated for the first group are very high in energy. At this high an energy it becomes questionable whether the shape of the potential energy curves can still be extrapolated precisely from only 6 to 8 data points around the optimal bond length. Interference of excited states may become an important factor at these energies. By running additional calculations at a wide variety of bond lengths may help to determine how much the potential energy curves are affected.

7 Summary and outlook

Current limits on the variation of two of the fundamental constants of the Standard Model are $\frac{\dot{\alpha}}{\alpha} < 5 \times 10^{-18} yr^{-1}$ for the fine structure constant and $\frac{\dot{\mu}}{\mu} = -0.2 \pm 1.1 \times 10^{-16} yr^{-1}$ for the proton-to-electron mass ratio. These limits are still consistent with a null hypothesis. More precise experiments are needed to constrain these limits even further.

In order to obtain precise experimental limits on the variation of fundamental constants sensitive probes are required. Which atoms or molecules are inherently sensitive to changes in the fundamental constants is not known but using advanced calculations it is possible to predict whether a system is likely to be sensitive. In these calculations one searches for quasi-degenerate transitions between levels of different nature, since these transitions provide highly sensitive probes.

Calculations of this kind were performed, and the results have been presented in this thesis. Two groups of molecules have been investigated using two different calculational methods: coupled cluster and configuration interaction. Both being suited for different kind of systems. All calculations have been performed using X2C Hamiltonians and had their energies converged with respect to the basis set.

For the first group, quasi-degenerate transitions were found by calculating the spectroscopic constants and reconstructing the potential energy curves, as well as the vibrational and rotational energy levels. Absolute and relative enhancement factors were determined. The highest absolute enhancement factors were found in the fine structure splitting of Sn_2^+ (both for μ and α). Due to a quasi-degenerate transition the relative enhancement was highest in the fine structure of Ge_2^+.

For the second group, quasi-degenerate transitions were already known from experiment beforehand so only the inherent sensitivity to α had to be determined. To this end α was varied directly in the calculations. The slope of transition energy as function of α then gives the enhancement factor. The highest enhancement factors for α were found transitions of SO^+ and Cl_2^+, whereas the O_2^+ proved to be highly sensitive to changes in μ.

Previous calculations for the enhancement factors for other molecules gave values that are comparable to the ones reported here. Only the most sensitive molecules in that work had higher enhancement factors. In an actual experiment the ease of cooling and trapping may prove to be more important than having the highest enhancement factors. This means that the most sensitive molecules reported here should definitely be added to the pool of molecules that should be considered for future experiments.

Further investigation on the presented molecules is advised if they are selected for actual experiment. There are three specific points of improvement that should be considered for further studies. The first would be using a wider scan of the potential energy curve of the first group of molecules to accommodate the vibrational levels with high energy. The second is an investigation into the energy levels of Cl_2^+, of which the calculated energies disagree with experiment.

Ultimately the results obtained in this work are very promising. A new selection of molecules has been shown to be sensitive to the variation of the fundamental constants α and μ. This

opens new possibilities when experiments are being set up. Even if none of the molecules end up being suited for experimental research, highly precise spectroscopic constants have still been obtained for molecules for which this information was previously unavailable.

8 Acknowledgements

I would like to deeply thank Dr. Anastasia Borschevsky for her excellent supervision. She taught me how to run calculations and, more importantly, helped me interpret the data (both the good and the bad). Additionally she allowed me to attend the Summerschool on physics beyond the Standard Model on Ameland, for which I am deeply grateful.

Also I thank Dr. Remco Havenith for allowing me to join in the group meetings and thus enabling me to get a taste of real science.

Special thanks to Lukáš Pašteka for providing the spectroscopic constants and energy curves for all the molecules in the second set.

References

[1] ATLAS Collaboration. Observation of a new particle in the search for the Standard Model Higgs boson with the ATLAS detector at the LHC. *Phys. Lett. B*, **716**:1 – 29, (2012).

[2] CMS Collaboration and LHCb Collaboration. Observation of the rare Bs0 $\rightarrow \mu^+\mu^-$decay from the combined analysis of CMS and LHCb data. *Nature*, **522**:68–72, (2015).

[3] Y. V. Stadnik and V. V. Flambaum. Manifestations of dark matter and variations of fundamental constants in atoms and astrophysical phenomena. *arXiv preprint: 1509.00966*, (2015).

[4] G. R. Farrar and M. E. Shaposhnikov. Baryon asymmetry of the universe in the minimal standard model. *Phys. Rev. Lett.*, **70**:2833–2836, (1993).

[5] S. M. Bilenky and S. T. Petcov. Massive neutrinos and neutrino oscillations. *Rev. Mod. Phys.*, **59**:671–754, (1987).

[6] J. Kersten and A. Y. Smirnov. Right-handed neutrinos at cern lhc and the mechanism of neutrino mass generation. *Phys. Rev. D*, **76**:073005, (2007).

[7] M. Dine. *Supersymmetry and string theory: Beyond the standard model.* (2016).

[8] G. Jungman, M. Kamionkowski, and K. Griest. Supersymmetric dark matter. *Phys. Rep.*, **267**:195 – 373, (1996).

[9] C. S. Aulakh and R. N. Mohapatra. Implications of supersymmetric so(10) grand unification. *Phys. Rev. D*, **28**:217–227, (1983).

[10] K. Hagiwara, K. Hikasa, K. Nakamura, M. Tanabashi, M. Aguilar-Benitez, et al. Review of particle physics. *Phys. Rev. D*, **66**:1, (2002).

[11] C. Giunti, C. W. Kim, and U. W. Lee. Running Coupling Constants and Grand Unification Models. *Mod. Phys. Lett. A*, **6**:1745–1755, (1991).

[12] M. Dine and A. Kusenko. Origin of the matter-antimatter asymmetry. *Rev. Mod. Phys.*, **76**:1–30, (2003).

[13] W. J. Marciano. Time variation of the fundamental "constants" and kaluza-klein theories. *Phys. Rev. Lett.*, **52**:489–491, (1984).

[14] J-P. Uzan. Varying constants, gravitation and cosmology. *Living Rev.Relat.*, **14**:2, (2011).

[15] V. V. Flambaum and E. V. Shuryak. Limits on cosmological variation of strong interaction and quark masses from big bang nucleosynthesis, cosmic, laboratory and oklo data. *Phys. Rev. D*, **65**:103503, (2002).

[16] V. V. Flambaum and E. V. Shuryak. Dependence of hadronic properties on quark masses and constraints on their cosmological variation. *Phys. Rev. D*, **67**:083507, (2003).

[17] R. M. Godun, P. B. R. Nisbet-Jones, J. M. Jones, S. A. King, L. A. M. Johnson, et al. Frequency Ratio of Two Optical Clock Transitions in $^{171}Yb^+$ and Constraints on the Time Variation of Fundamental Constants. *Phys. Rev. Lett.*, **113**:210801, (2014).

[18] P. A. M. Dirac. The cosmological constants. *Nature*, **139**:323, (1937).

[19] A. I. Shlyakhter. Direct test of the constancy of fundamental nuclear constants. *Nature Lett.*, **264**:340, (1976).

[20] P. A. R. Ade, N. Aghanim, M. Arnaud, et al. Planck intermediate results - XXIV. Constraints on variations in fundamental constants. *A&A*, **580**:A22, (2015).

[21] P. A. R. Ade, N. Aghanim, M. Arnaud, M. Ashdown, J. Aumont, et al. Planck 2015 results-XIII. Cosmological parameters. *A&A*, **594**:A13, (2016).

[22] M. T. Murphy, J. K. Webb, and V. V. Flambaum. Further evidence for a variable fine-structure constant from Keck/HIRES QSO absorption spectra. *Mon. Not. R. Astron. Soc.*, **345**:609–638, 2003.

[23] T. Lenoir. Practice, reason, context: The dialogue between theory and experiment. *Sci. Context*, **2**:3– 22, (1988).

[24] E. D. Davis, C. R. Gould, and E. I. Sharapov. Oklo reactors and implications for nuclear science. *Int. J. Mod. Phys. E*, **23**:1430007, (2014).

[25] T. Damour and F. Dyson. The oklo bound on the time variation of the fine-structure constant revisited. *Nucl. Phys. B*, **480**:37 – 54, (1996).

[26] E. D. Davis and L. Hamdan. Reappraisal of the limit on the variation in α implied by the oklo natural fission reactors. *Phys. Rev. C*, **92**:014319, (2015).

[27] J. Terrien. News from the International Bureau of Weights and Measures. *Metrologia*, **4**:41–45, (1968).

[28] H. Marion, F. Pereira Dos Santos, M. Abgrall, S. Zhang, Y. Sortais, et al. Search for variations of fundamental constants using atomic fountain clocks. *Phys. Rev. Lett.*, **90**:150801, (2003).

[29] M. P. Savedoff. Physical constants in extra-galactic nebulae. *Nature*, **178**:688–689, (1956).

[30] John K. Webb, Victor V. Flambaum, Christopher W. Churchill, Michael J. Drinkwater, and John D. Barrow. Search for time variation of the fine structure constant. *Phys. Rev. Lett.*, **82**:884–887, 1999.

[31] L. L. Cowie and A. Songaila. Astrophysical limits on the evolution of dimensionless physical constants over cosmological time. *Astrophys. J.*, **453**:596, (1995).

[32] P. Tzanavaris, J. K. Webb, M. T. Murphy, V. V. Flambaum, and S. J. Curran. Limits on variations in fundamental constants from 21-cm and ultraviolet quasar absorption lines. *Phys. Rev. Lett.*, **95**:041301, (2005).

[33] V. A. Dzuba, V. V. Flambaum, and J. K. Webb. Calculations of the relativistic effects in many-electron atoms and space-time variation of fundamental constants. *Phys. Rev. A*, **59**:230, (1999).

[34] H. Chand, R. Srianand, P. Petitjean, and B. Aracil. Probing the cosmological variation of the fine-structure constant: Results based on VLT-UVES sample . *A&A*, **417**:853–871, (2004).

[35] M. T. Murphy, J. K. Webb, and V. V. Flambaum. Comment on limits on the time variation of the electromagnetic fine-structure constant in the low energy limit from absorption lines in the spectra of distant quasars. *Phys. rev. lett.*, **99**:239001, (2007).

[36] J. K. Webb, J. A. King, M. T. Murphy, V. V. Flambaum, R. F. Carswell, and M. B. Bainbridge. Indications of a spatial variation of the fine structure constant. *Phys. Rev. Lett.*, **107**:191101, (2011).

[37] J. A. King, J. K. Webb, M. T. Murphy, V. V. Flambaum, R. F. Carswell, et al. Spatial variation in the fine-structure constant new results from VLT/UVES. *Mon. Not. R. Astron. Soc.*, **422**:3370, (2012).

[38] J. C. Berengut and V. V. Flambaum. Manifestations of a spatial variation of fundamental constants in atomic and nuclear clocks, oklo, meteorites, and cosmological phenomena. *Europhys. Lett.*, **97**:20006, (2012).

[39] A. Songaila and L. L. Cowie. Constraining the variation of the fine-structure constant with observations of narrow quasar absorption lines. *Astrophys. J.*, **793**:103, (2014).

[40] J. Bagdonaite, P. Jansen, C. Henkel, H. L. Bethlem, K. M. Menten, et al. A stringent limit on a drifting proton-to-electron mass ratio from alcohol in the early universe. *Science*, **339**:46–48, (2013).

[41] J. Bagdonaite, W. Ubachs, M. T. Murphy, and J. B. Whitmore. Constraint on a varying proton-electron mass ratio 1.5 billion years after the big bang. *Phys. Rev. Lett.*, **114**:071301, (2015).

[42] C. Chin, V. V. Flambaum, and M. G. Kozlov. Ultracold molecules: new probes on the variation of fundamental constants. *New J. Phys.*, **11**:055048, (2009).

[43] A. Shelkovnikov, R. J. Butcher, C. Chardonnet, and A. Amy-Klein. Stability of the proton-to-electron mass ratio. *Phys. Rev. Lett.*, **100**:150801, (2008).

[44] E. R. Hudson, H. J. Lewandowski, B. C. Sawyer, and J. Ye. Cold molecule spectroscopy for constraining the evolution of the fine structure constant. *Phys. Rev. Lett.*, **96**:143004, (2006).

[45] L. F. Pašteka, A. Borschevsky, V. V. Flambaum, and P. Schwerdtfeger. Search for the variation of fundamental constants: Strong enhancements in $X\ ^2\Pi$ cations of dihalogens and hydrogen halides. *Phys. Rev. A*, **92**:012103, (2015).

[46] K. Beloy, A. Borschevsky, V. V. Flambaum, and P. Schwerdtfeger. Effect of α variation on a prospective experiment to detect variation of $\mathrm{m}_e/\mathrm{m}_p$ in diatomic molecules. *Phys. Rev. A*, **84**:042117, (2011).

[47] K. Beloy, M. G. Kozlov, A. Borschevsky, A. W. Hauser, V. V. Flambaum, and P. Schwerdtfeger. Rotational spectrum of the molecular ion NH^+ as a probe for α and $\mathrm{m}_e/\mathrm{m}_p$ variation. *Phys. Rev. A*, **83**:062514, (2011).

[48] K. Beloy, A. W. Hauser, A. Borschevsky, V. V. Flambaum, and P. Schwerdtfeger. Effect of α variation on the vibrational spectrum of Sr_2. *Phys. Rev. A*, **84**:062114, (2011).

[49] V. V. Flambaum and M. G. Kozlov. Enhanced sensitivity to the time variation of the fine-structure constant and m_p/m_e in diatomic molecules. *Phys. Rev. Lett.*, **99**:150801, (2007).

[50] K. Beloy, A. Borschevsky, P. Schwerdtfeger, and V. V. Flambaum. Enhanced sensitivity to the time variation of the fine-structure constant and m_p/m_e in diatomic molecules: A closer examination of silicon monobromide. *Phys. Rev. A*, **82**:022106, (2010).

[51] R. F. Bishop and H. G. Kümmel. The coupled cluster method. *Phys. Today*, **40**:52–60, (1987).

[52] D. Cremer. From configuration interaction to coupled cluster theory: The quadratic configuration interaction approach. *Wiley Interdiscip. Rev. Comput. Mol. Sci.*, **3**:482–503, (2013).

[53] R. Bast, T. Saue, L. Visscher, H. J. A. Jensen, et al., (2015). DIRAC, a relativistic ab initio electronic structure program.

[54] H. J. Werner, P. J. Knowles, G. Knizia, F. R. Manby, M. Schütz, et al. Molpro, version 2015.1, a package of ab initio programs.

[55] GAMESS-UK is a package of ab initio programs. See: http://www.cfs.dl.ac.uk/gamess-uk/index.shtml, M.F. Guest, I. J. Bush, H.J.J. van Dam, P. Sherwood, J.M.H. Thomas, J.H. van Lenthe, R.W.A Havenith, J. Kendrick, The GAMESS-UK electronic structure package: algorithms, developments and applications, Molecular Physics, Vol. 103, No. 6-8, 20 March-20 April 2005, 719-747.

[56] K. S. Pitzer. Relativistic effects on chemical properties. *Acc. Chem. Res.*, **12**:271–276, (1979).

[57] T. Saue. Relativistic hamiltonians for chemistry: A primer. *ChemPhysChem*, **12**:3077–3094, (2011).

[58] K. G. Dyall. Interfacing relativistic and nonrelativistic methods. i. normalized elimination of the small component in the modified dirac equation. *J. Chem. Phys.*, **106**(23), (1997).

[59] Iliaš, M. and Jensen, H. J. A. and Kellö, V. and Roos, B. O. and Urban, M. Theoretical study of PbO and the PbO anion. *Chem. Phys. Lett.*, **408**:210 – 215, (2005).

[60] P. W. Atkins and R. S. Friedman. *Molecular quantum mechanics.* (2011).

[61] R. J. Bartlett and M. Musiał. Coupled-cluster theory in quantum chemistry. *Rev. Mod. Phys.*, **79**:291–352, (2007).

[62] C. D. Sherrill. An introduction to hartree-fock molecular orbital theory. *Georgia inst. of technology, unpublished*, (2000).

[63] T. Tsuneda. *Density functional theory in quantum chemistry.* (2014).

[64] C. D. Sherrill. An introduction to configuration interaction theory. *Georgia inst. of technology, unpublished*, (1995).

[65] I.N. Levine. *Quantum Chemistry.* (2013).

[66] E. R. Davidson and D. Feller. Basis set selection for molecular calculations. *Chem. Rev.*, **86**:681–696, (1986).

[67] A. C. Tsipis. DFT assessment of the spectroscopic constants and absorption spectra of neutral and charged diatomic species of group 11 and 14 elements. *J. Comput. Chem.*, **35**:1762–1777, (2014).

[68] T. Zeng, D. G. Fedorov, and M Klobukowski. Model core potentials of p-block elements generated considering the Douglas-Kroll relativistic effects, suitable for accurate spin-orbit coupling calculations. *J. Chem. Phys.*, **133**:114107, (2010).

[69] T. Zeng, D. G. Fedorov, and M. Klobukowski. Performance of dynamically weighted multiconfiguration self-consistent field and spin-orbit coupling calculations of diatomic molecules of group 14 elements. *J. Chem. Phys.*, **134**:024108, (2011).

[70] S Chattopadhyaya and K. K. Das. Electronic spectrum of $SiSe^+$: a MRDCI study. *Chem. Phys. Lett.*, **399**:140 – 146, (2004).

[71] S. Chattopadhyaya, A. Pramanik, A. Banerjee, and K. K. Das. Electronic States and Spectroscopic Properties of SiTe and SiTe+. *J. Phys. Chem. A*, **110**:12303–12311, (2006).

[72] K. Balasubramanian. Relativistic Configuration Interaction Calculations of Low-Lying States of SnO^+, PbO^+, PbS^+, and $PbSe^+$. Comparison with the Photoelectron Spectra of SnO. *J.Phys. Chem.*, **88**, (1984).

[73] V. E. Jackson, D. A. Dixon, and K. O. Christe. Thermochemical properties of selenium fluorides, oxides, and oxofluorides. *Inorg. Chem.*, **51**:2472–2485, (2012).

[74] J. A. Coxon, S. Naxakis, and A. Brian Yamashita. First observation of the SeO^+ emission spectrum vibrational analysis of the $A^2\Pi - X^2\Pi$ system. *Chem. Phys. Lett.*, **117**, (1985).

[75] L.-S. Wang, Y. T. Lee, D. A. Shirley, K. Balasubramanian, and P. Feng. Photoelectron spectroscopy and electronic structure of clusters of the group v elements. i. dimers. *J. Chem. Phys.*, **93**:6310–6317, (1990).

[76] Pašteka Lukáš F.; Comenius university Bratislava. private communication.

[77] K. Beloy, A. Borschevsky, P. Schwerdtfeger, and V. V. Flambaum. Enhanced sensitivity to the time variation of the fine-structure constant and m_p/m_e in diatomic molecules: A closer examination of silicon monobromide. *Phys. Rev. A*, **82**:022106, (2010).

[78] Iliaš, M. and Saue, T. An infinite-order two-component relativistic hamiltonian by a simple one-step transformation. *J. Chem. Phys.*, **126**:064102, (2007).

[79] A. K. Wilson, D. E. Woon, K. A. Peterson, and T. H. Dunning Jr. Gaussian basis sets for use in correlated molecular calculations. IX. The atoms gallium through krypton. *J. Chem. Phys.*, **110**:7667–7676, (1999).

[80] K. G. Dyall. *Theor. Chem. Acc.*, **115**:441, (2006).

[81] V. Kellö; Comenius University. *unpublished*.

[82] J. L. Dunham. The energy levels of a rotating vibrator. *Phys. Rev.*, **41**:721, (1932).

[83] J. L. Dunham. The Wentzel-Brillouin-Kramers method of solving the wave equation. *Phys. Rev.*, **41**(6):713, (1932).

[84] T. Fleig. *Wave Function Based Relativistic Multi-Reference Electron Correlation Methods. Development and Application to Atomic and Molecular Properties.* PhD thesis, (2006).

[85] J. H. Van Vleck. On σ-type doubling and electron spin in the spectra of diatomic molecules. *Phys. Rev.*, **33**:467–506, (1929).

[86] R. S. Mulliken and A. Christy. Λ. *Phys. Rev.*, **38**:87–119, (1931).

[87] S. Mollet and F. Merkt. The $X^{+2}\Pi_g, A^{+2}\Pi_u, B^{+2}\Delta_u$, and $a^{4+}\Sigma_u$ electronic states of Cl_2^+ studied by high-resolution photoelectron spectroscopy. *J. Chem. Phys.*, **139**, (2013).

[88] M. A. Gharaibeh, D. J. Clouthier, A. Kalemos, H. Lefebvre-Brion, and R. W. Field. A new, definitive analysis of a very old spectrum: The highly perturbed $A^2\Pi_u \rightarrow X^2\Pi_g$ band system of the chlorine cation (Cl_2^+). *J. Chem. Phys.*, **137**:137, (2012).

[89] I. W. Milkman, J. C. Choi, J. L. Hardwick, and J. T. Moseley. High-resolution studies of the $A^2\Pi \rightarrow X^2\Pi$ system of rotationally cooled SO^+. *J. Mol. Spectros.*, **130**:20 – 32, (1988).

[90] D. Cossart, D Lavendy, and J. M. Robbe. The first valence states of the SO^+ ion. *J. Mol. Spectros.*, **99**:369 – 406, (1983).

[91] C.V.V. Prasad, D. Lacombe, K. Walker, W. Kong, P. Bernath, and J. Hepburn. Fourier transform emission spectroscopy of the second negative ($A^2\Pi_u$-$X^2\Pi_g$) system of the O_2^+ ion. *Mol. Phys.*, **91**:1059–1074, (1997).

[92] R. R. Laher and F. R. Gilmore. Improved fits for the vibrational and rotational constants of many states of nitrogen and oxygen. *J. Phys. Chem. Ref. Data*, **20**:685–712, (1991).

[93] W. Kong and J. W. Hepburn. Rotationally resolved threshold photoelectron spectroscopy of O_2 using coherent XUV: formation of vibrationally excited ions in the FranckâĂŞCondon gap. *Can. J. Phys.*, **72**:1284–1293, (1994).

[94] J. A. Coxon and M. P. Haley. Rotational analysis of the $A^2\Pi_u \rightarrow X^2\Pi_g$ second negative band system of $^{16}O_2^+$. *J. Mol. Spectros.*, **108**:119 – 136, (1984).

[95] P. C. Cosby, J. B. Ozenne, J. T. Moseley, and D. L. Albritton. High-resolution photofragment spectroscopy of the o_2^+ $b^4\sigma_g$ (vâĂš = 3, 4, 5) $\leftarrow$ $a^4\pi_u$ (vâĂš = 3, 4, 5) first negative system using coaxial dye-laser and velocity-tuned ion beams. *J. Mol. Spectros.*, **79**:203 – 235, (1980).

[96] K. Brabaharan and J. A. Coxon. Rotational analysis of the $A^2\Pi_u \rightarrow X^2\Pi_g$ system of $^{32}S_2^+$. *J. Mol. Spectros.*, **128**:540 – 553, 1988.

[97] J. P. Maier and M. Rösslein. The $B^4\Sigma_u \rightarrow X^4\Sigma_g$ electronic spectrum of C_2^+. *J.Chem. Phys.*, **88**:4614–4620, (1988).

9 Appendix A

Table 7: General active spaces used in the CI calculations. Orbitals are frozen from the core outwards.

Molecule	Number of electrons	Frozen orbitals	Active orbitals
Cl_2^+	31	11	10
C_2^+	11	0	10
O_2^+	15	2	8
SO^+	23	9	6

10 Appendix B

Table 8: Spectroscopic constants for $^{74}Ge_2^+$, mass: 73.921177 u

Method	FSCC		CCSD		CCSD(T)		Corrected FSCC		Other	source
State	$\Pi_{1/2}$	$\Pi_{3/2}$	$\Pi_{1/2}$	$\Pi_{3/2}$	$\Pi_{1/2}$	$\Pi_{3/2}$	$\Pi_{1/2}$	$\Pi_{3/2}$	$\Pi_{1/2}$	$\Pi_{3/2}$
R_e (Å)	2.577	2.577	2.558	2.558	2.576	2.575	2.581	2.582	2.407	2.407
B_e (cm^{-1})	0.0687	0.0687	0.0697	0.0697	0.0687	0.0688	0.0684	0.0684		
$\alpha_e \times 10^4$ (cm^{-1})	2.425	2.392	2.071	1.849	2.227	2.152	2.301	2.316		
ω_e (cm^{-1})	230.0	231.0	238.8	241.1	229.1	230.5	226.65	226.68	209	209
$\omega_e x_e$ (cm^{-1})	0.41	0.41	0.83	0.83	1.0	0.96	1.04	1.04	0.61	0.56
$D_e \times 10^8$ (cm^{-1})	2.448	2.429	2.373	2.329	2.477	2.452	2.496	2.495		
$\beta_e \times 10^{10}$ (cm^{-1})	-1.284	-1.118	2.742	3.097	4.254	3.982	4.628	4.563		
A_e (cm^{-1})	857.4		930.7		914.9		862.3			

Table 9: Spectroscopic constants for $^{74}As_2^+$, mass: 74.921594 u gs: $\Pi_{3/2}$

Method	FSCC		CCSD		CCSD(T)		Corrected FSCC		Other	source
State	$\Pi_{1/2}$	$\Pi_{3/2}$	$\Pi_{1/2}$	$\Pi_{3/2}$	$\Pi_{1/2}$	$\Pi_{3/2}$	$\Pi_{1/2}$	$\Pi_{3/2}$	$\Pi_{1/2}$	$\Pi_{3/2}$
R_e (Å)	2.162	2.162	2.176	2.176	2.195	2.194	2.181	2.180	2.231	2.230
B_e (cm^{-1})	0.0962	0.0963	0.0950	0.0951	0.0934	0.0934	0.0946	0.0947		
$\alpha_e \times 10^4$ (cm^{-1})	2.831	2.835	2.825	2.723	3.551	3.552	3.022	3.020		
ω_e (cm^{-1})	415.00	414.75	400.79	400.03	378.58	378.66	394.02	393.93	380	385
$\omega_e x_e$ (cm^{-1})	0.828	0.826	6.44	4.72	1.35	1.40	0.810	0.807		
$D_e \times 10^8$ (cm^{-1})	2.071	2.078	2.136	2.147	2.271	2.276	2.183	2.189		
$\beta_e \times 10^{10}$ (cm^{-1})	-0.609	-0.711	-0.761	-1.359	1.605	1.847	-0.282	-0.2906		
A_e (cm^{-1})	1403.49		1391.8		1375.7		1379.8			

Table 10: Spectroscopic constants for $^{120}Sn_2^+$, mass: 119.902220 u gs: $\Pi_{1/2}$

Method	FSCC		CCSD		CCSD(T)		Corrected FSCC		Other	source
State	$\Pi_{1/2}$	$\Pi_{3/2}$	$\Pi_{1/2}$	$\Pi_{3/2}$	$\Pi_{1/2}$	$\Pi_{3/2}$	$\Pi_{1/2}$	$\Pi_{3/2}$	$\Pi_{1/2}$	$\Pi_{3/2}$
R_e (Å)	2.935	2.931	2.944	2.926	2.962	2.947	2.952	2.954	2.624^{a*} 3.080^{b*} 3.046^{c*} 2.923^{j*}	2.772^{a*} 3.073^{b*} 3.045^{c*} 2.914^{j*}
B_e (cm^{-1})	0.0327	0.0327	0.0324	0.0328	0.0321	0.0324	0.0323	0.0322		
$\alpha_e \times 10^5$ (cm^{-1})	8.061	7.662	9.235	6.992	9.188	7.617	7.466	8.09		
ω_e (cm^{-1})	160.6	163.5	154.8	165.2	149.6	157.2	155.4	154.6	160.5^{a*} 132^{b*} 143^{c*} 159^{j*}	173.9^{a*} 135^{b*} 143^{c*} 158^{j*}
$\omega_e x_e$ (cm^{-1})	0.34	0.32	0.45	0.28	0.40	0.32	0.26	0.33	0.34^{b*} 0.31^{j*}	0.35^{b*} 0.31^{j*}
$D_e \times 10^9$ (cm^{-1})	5.400	5.253	5.703	5.194	5.886	5.492	5.559	5.607		
$\beta_e \times 10^{11}$ (cm^{-1})	1.736	1.496	4.254	1.112	3.175	1.768	0.305	1.857		
A_e (cm^{-1})	2269.3		2524.0		2419.6		2157.1		2101^{j*}	

Reference a* finds the Σ state as the ground state. In this case, replace $\Pi_{1/2}$ and $\Pi_{3/2}$ by $^4\Sigma_{g^-}$ and $^2\Sigma_{g^+}$ respectively.

Table 11: Spectroscopic constants for $^{208}Pb^{32}S^{+}$, masses: 207.976627 and 31.97207 u gs: $\Pi_{3/2}$

Method	FSCC		CCSD		CCSD(T)		Corrected FSCC		Other	source
State	$\Pi_{1/2}$	$\Pi_{3/2}$	$\Pi_{1/2}$	$\Pi_{3/2}$	$\Pi_{1/2}$	$\Pi_{3/2}$	$\Pi_{1/2}$	$\Pi_{3/2}$	$\Pi_{1/2}$	$\Pi_{3/2}$
R_e (Å)	2.405	2.409	2.427	2.434	2.434	2.444	2.405	2.409	2.56	2.56
B_e (cm^{-1})	0.105	0.105	0.103	0.103	0.103	0.102	0.105	0.105		
ω_e (cm^{-1})	383.1	405.0	347.0	357.8	339.1	348.4	383.1	405.0	335	363
$\omega_e x_e$ (cm^{-1})	1.541	2.078	0.785	0.855	1.158	1.086	1.541	2.078		
$\alpha_e \times 10^4$ (cm^{-1})	6.328	6.725	2.599	3.701	2.712	4.071	6.324	6.725		
$D_e \times 10^8$ (cm^{-1})	3.167	2.809	3.662	3.385	3.765	3.485	3.167	2.809		
$\beta_e \times 10^9$ (cm^{-1})	-0.107	0.0661	0.170	-0.0262	0.495	0.0932	-0.107	0.0661		
A_e (cm^{-1})	796.2		1035.9		1082.8		797.4		506	

11 Appendix C

Figure 9: Potential energy curves of the fine structure of Ge_2^+ (left) and As_2^+ (right). Vibrational levels have been added and quasi-degenerate levels are indicated with an arrow.

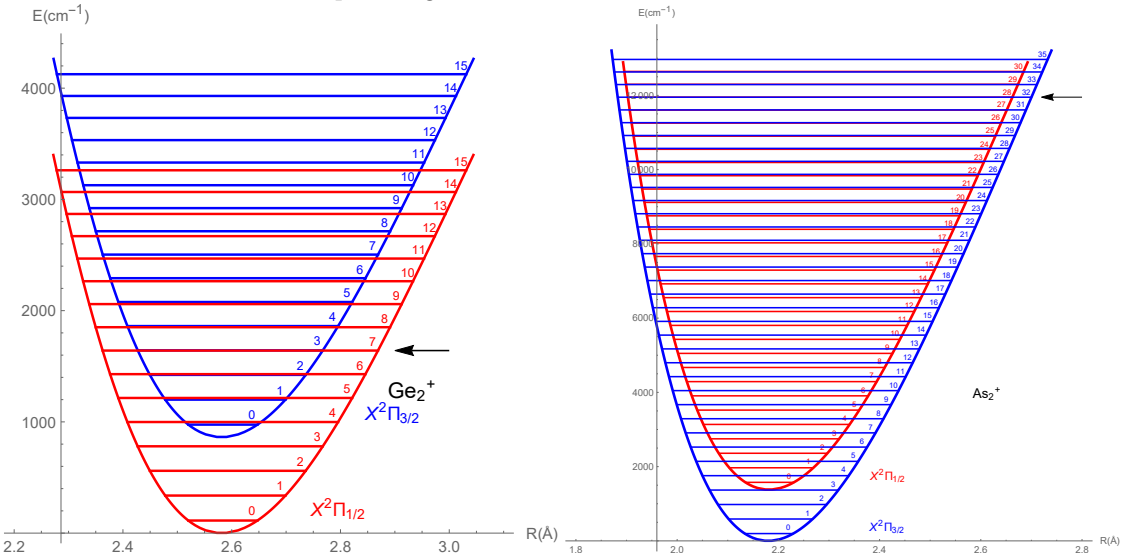

Figure 10: Potential energy curves of the fine structure of Sn_2^+ (left) and PbS^+ (right). Vibrational levels have been added and quasi-degenerate levels are indicated with an arrow.

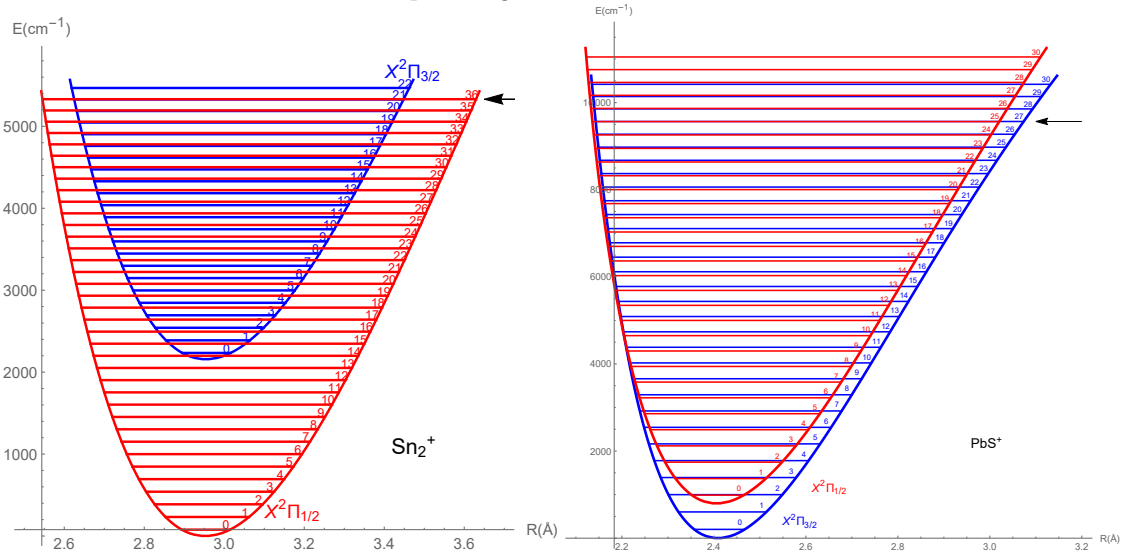

12 Appendix D

Figure 11: Rotational energy levels and their transition energies for Sn_2^+ (left) and PbS^+ (right)

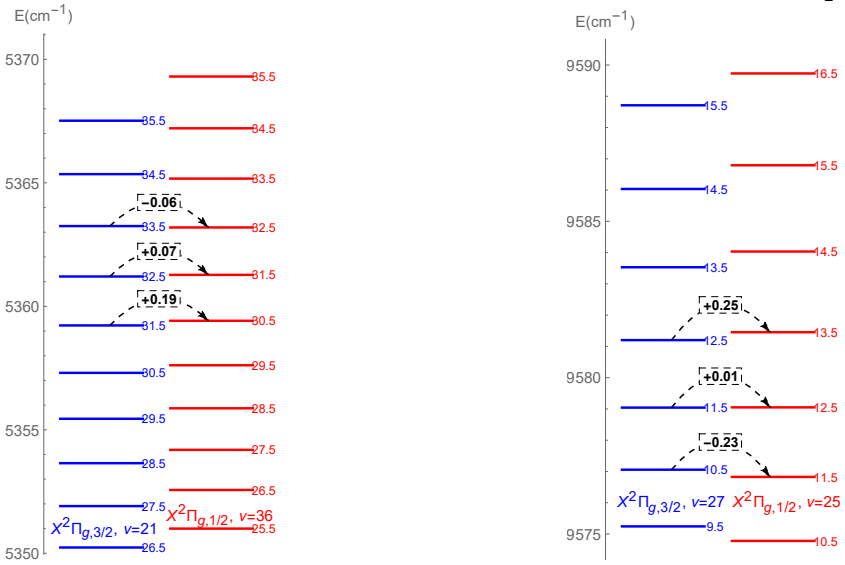

Figure 12: Rotational energy levels and their transition energies for Ge_2^+ (left) and As_2^+ (right)

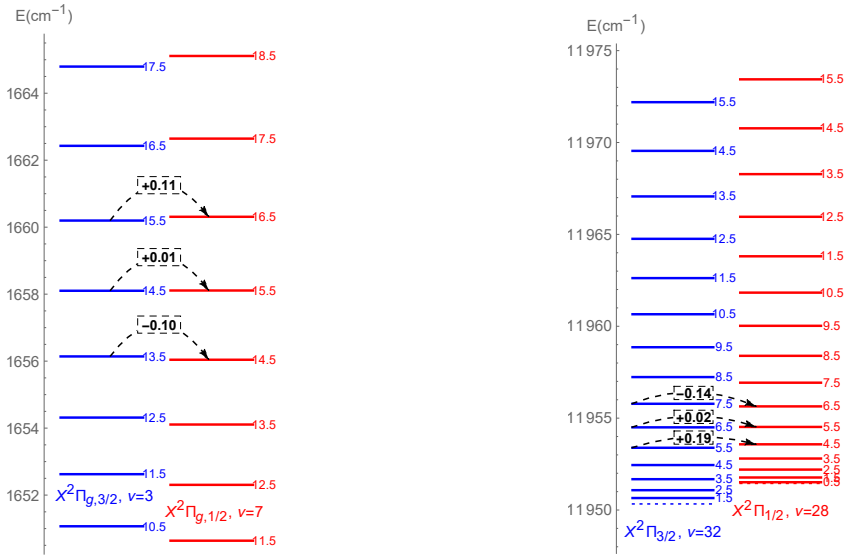

13 Appendix E

Equation 30 gives the enhancement factor of a transition as function of the spectroscopic constants of a molecule. It does not, however, take into account that the spectroscopic constants differ slightly between the levels of the transition. In the tables in this appendix the enhancement factors are evaluated using different combinations of the spectroscopic constants. Included are: $X\Pi_{1/2}$ only, $X\Pi_{3/2}$ only, the average of those two and a combination of the two. This last version of equation 30 is given by:

$$K_\mu = \tfrac{1}{2}\omega_{e,2}\nu_2 - \tfrac{1}{2}\omega_{e,1}\nu_1 + \omega_e x_{e,1}(\nu_1^2 + \nu_1) - \omega_e x_{e,2}(\nu_2^2 + \nu_2) \quad (36)$$

$$+B_{e,2}(J_2^2 + J_2) - B_{e,1}(J_1^2 + J_1) \quad (37)$$

Table 12: Enhancement factors Sn_2^+, corrected FSCC calculations. $\Pi_{3/2}$ is v".

Notes	ν"	ν'	J"	J'	ω	$\bar{K}_\mu$	K_μ	$\bar{K}_\alpha$	K_α
$X\Pi_{1/2}$									
constants	21	36	31.5	30.5	0.18	-940.7	-5226.4	-4314.2	-23968.0
			32.5	31.5	0.06	-940.7	-15678.1	-4314.2	-71904.1
			33.5	32.5	-0.06	-940.6	15677.0	-4314.2	71904.1
$X\Pi_{3/2}$									
constants	21	36	31.5	30.5	0.18	-869.5	-4830.6	-4314.2	-23968.0
			32.5	31.5	0.06	-869.4	-14490.6	-4314.2	-71904.1
			33.5	32.5	-0.06	-869.4	14489.5	–4314.2	71904.1
Average enhancement									
factors	21	36	31.5	30.5	0.18	-905.1	-5028.5	-4314.2	-23968.0
			32.5	31.5	0.06	-905.1	-15084.3	-4314.2	-71904.1
			33.5	32.5	-0.06	-905.0	15083.2	-4314.2	71904.1
Combined									
constants	21	36	31.5	30.5	0.18	-983.8	-5465.7	-4314.2	-23968.0
			32.5	31.5	0.06	-983.8	-16396.1	-4314.2	-71904.1
			33.5	32.5	-0.06	-983.7	16395.1	-4314.2	71904.1

Table 13: Enhancement factors Ge_2^+, corrected FSCC calculations. $\Pi_{3/2}$ is v".

Notes	ν"	ν'	J"	J'	ω	$\bar{K}_\mu$	K_μ	$\bar{K}_\alpha$	K_α
$X\Pi_{1/2}$									
constants	3	7	13.5	14.5	-0.1	-409.3	4092.7	-1724.6	17245.8
			14.5	15.5	0.01	-409.4	-40940.6	-1724.6	-172458.5
			15.5	16.5	0.11	-409.5	-3723.1	-1724.6	-15678.0
$X\Pi_{3/2}$									
constants	3	7	13.5	14.5	-0.1	-409.3	4092.7	-1724.6	17245.8
			14.5	15.5	0.01	-409.5	-40940.6	-1724.6	-172458.5
			15.5	16.5	0.11	-409.8	-3723.1	-1724.6	-15678.0
Average enhancement									
factors	3	7	13.5	14.5	-0.1	-409.4	4092.7	-1724.6	17245.8
			14.5	15.5	0.01	-409.5	-40940.6	-1724.6	-172458.5
			15.5	16.5	-0.11	-409.7	-3723.1	-1724.6	-15678.0
Combined									
constants	3	7	13.5	14.5	-0.1	-409.2	4091.8	-1724.6	17245.8
			14.5	15.5	0.01	-409.3	-40931.8	-1724.6	-172458.5
			15.5	16.5	0.11	-409.5	-3722.3	-1724.6	-15678.0

Table 14: Enhancement factors As_2^+, corrected FSCC calculations. $\Pi_{3/2}$ is v".

Notes	ν"	ν'	J"	J'	ω	$\bar{K}_\mu$	K_μ	$\bar{K}_\alpha$	K_α
$X\Pi_{1/2}$									
constants	32	28	5.5	4.5	0.19	591.4	3112.8	-2759.7	-14524.5
			6.5	5.5	0.02	591.6	29581.5	-2759.7	-137982.9
			7.5	6.5	-0.14	591.8	-4227.3	-2759.7	19711.8
$X\Pi_{3/2}$									
constants	32	28	5.5	4.5	0.19	591.9	3115.2	-2759.7	-14524.5
			6.5	5.5	0.02	591.6	29581.5	-2759.7	-137982.9
			7.5	6.5	-0.14	591.8	-4227.3	-2759.7	19711.8
Average enhancement									
factors	32	28	5.5	4.5	0.19	591.4	3112.8	-2759.7	-14524.5
			6.5	5.5	0.02	591.6	29581.5	-2759.7	-137982.9
			7.5	6.5	-0.14	591.8	-4227.3	-2759.7	19711.8
Combined									
constants	32	28	5.5	4.5	0.19	592.8	3120.1	-2759.7	-14524.5
			6.5	5.5	0.02	592.9	29643.8	-2759.7	-137982.9
			7.5	6.5	-0.14	592.9	-4235.1	-2759.7	19711.8

Table 15: Enhancement factors PbS^+, corrected FSCC calculations. $\Pi_{3/2}$ is v".

Notes	ν"	ν'	J"	J'	ω	$\bar{K}_\mu$	K_μ	$\bar{K}_\alpha$	K_α
$X\Pi_{1/2}$ constants	27	25	10.5	11.5	-0.23	217.3	-945.0	-1594.9	6934.2
			11.5	12.5	0.01	217.1	21712.9	-1594.9	-159487.4
			12.5	13.5	0.25	216.9	867.7	-1594.9	-6379.5
$X\Pi_{3/2}$ constants	27	25	10.5	11.5	-0.23	182.3	-792.7	-1594.9	6934.2
			11.5	12.5	0.01	182.1	18210.7	-1594.9	-159487.4
			12.5	13.5	0.25	181.9	727.6	-1594.9	6379.5
Average enhancement factors	27	25	10.5	11.5	-0.23	199.8	-868.8	-1594.9	6934.2
			11.5	12.5	0.01	199.6	19961.8	-1594.9	-159487.4
			12.5	13.5	0.25	199.4	797.6	-1594.9	6379.5
Combined constants	27	25	10.5	11.5	-0.23	107.0	-465.3	-1594.9	6934.2
			11.5	12.5	0.01	106.8	10680.7	-1594.9	-159487.4
			12.5	13.5	0.25	106.6	426.4	-1594.9	6379.5

14 Appendix F

Table 16: Spectroscopic constants of Cl_2^+. a from [87]; b from [88].

constant	$X^2\Pi^a_{g,3/2}$	$X^2\Pi^a_{g,1/2}$	$a^4\Sigma^{a,-}_{u,1/2}$	$a^4\Sigma^{a,-}{}_{u,3/2}$	$A^2\Pi^b_{u,3/2}$	$B^2\Delta^b_{u,3/2}$
T_e (cm^{-1})	0	717.5	17114.1	17151.6	20440.81	21913.42
ω_e (cm^{-1})	645.97	645.26	329.1	329.7	386.46	284.49
$\omega_e x_e$ (cm^{-1})	3.10	3.10	1.743	1.722	2.027	1.533
$\omega_e y_e$ (cm^{-1})	0.0078	0.0075			-0.0299	-0.0094
$\omega_e z_e \times 10^4$ (cm^{-1})	1.25	1.30			10.10	1.57
B_e (cm^{-1})	0.2707	0.2699	0.175	0.175	0.18975	0.16174
$\alpha_e \times 10^3$ (cm^{-1})	1.2	1.5			1.3759	1.1933

Figure 13: Rotational transitions in Cl_2^+. Of interest are the degenerate levels $X^2\Pi_{g,3/2}$ (42,9.5) and $a^4\Sigma^-_{u,1/2}$ (19,8.5))

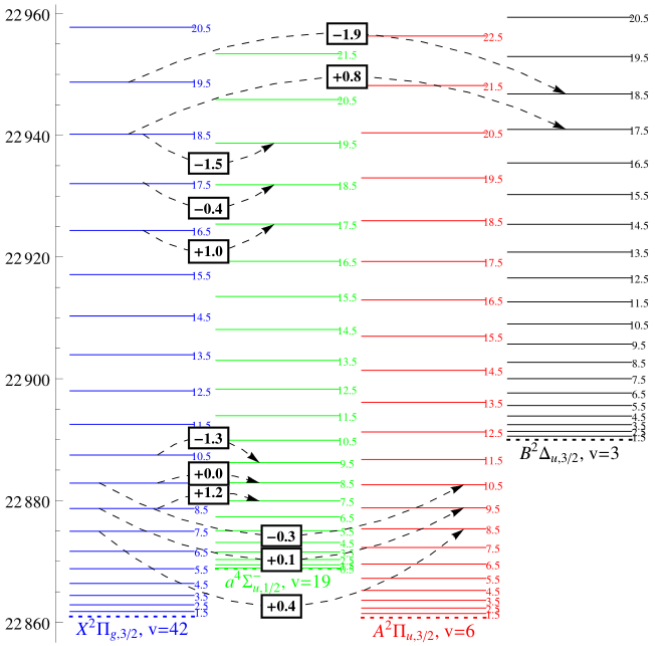

Table 17: Spectroscopic constants of SO^+. a from [89]; b from [90].

constant	$X^2\Pi^a$	$A^2\Pi^a$	$a^4\Pi^b$
T_e (cm^{-1})	0	31421.49	25474
ω_e (cm^{-1})	1306.778	805.594	884
$\omega_e x_e$ (cm^{-1})	7.6975	13.574	6.8
$\omega_e y_e$ (cm^{-1})	-0.0019	-0.0031	
$\omega_e z_e$ (cm^{-1})		0.00109	
B_e (cm^{-1})	0.7785924	0.575344	0.578
$\alpha_e \times 10^3$ (cm^{-1})	6.21	5.9137	
$D_e \times 10^6$ (cm^{-1})	1.10557	1.17384	0.98841
A_e (cm^{-1})	364.38	-53.88	-61.2
$A_\nu^{(1)}$ (cm^{-1})	-0.404	0.612	
$A_\nu^{(2)}$ (cm^{-1})	-0.0374	0.0485	

Figure 14: Rotational states in SO^+ including the transition belonging to the highest relative enhancement factor.

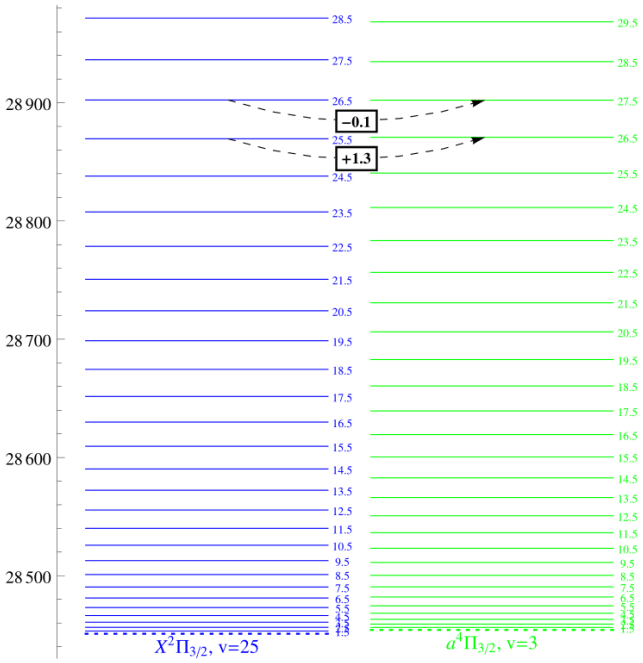

Table 18: Spectroscopic constants of O_2^+. a from [91], b from [92], c from [93], d from a fit through the data in [94] and e from [95].

constant	$X^2\Pi^a$	$A^2\Pi^a$	$a^4\Pi^b$
T_e (cm^{-1})	0	40572.785	32962.2
ω_e (cm^{-1})	1905.892	898.65	1035.13
$\omega_e x_e$ (cm^{-1})	16.489	13.574	10.115
$\omega_e y_e$ (cm^{-1})	0.02057	-0.0066	-0.0331
B_e (cm^{-1})	1.689824	1.061939	1.10476
$\alpha_e \times 10^2$ (cm^{-1})	1.9363	1.9598	0.01548
$\gamma_e \times 10^5$ (cm^{-1})	-1.32	-10.19	1.2
$D_e \times 10^6$ (cm^{-1})	5.31359	5.93168	5.0954
A_e (cm^{-1})	200.681 [c]	-3.297[d]	-47.78535[e]
$A_\nu^{(1)}$ (cm^{-1})	-0.648[c]	-0.154[d]	-0.01860[e]
$A_\nu^{(2)}$ (cm^{-1})	-0.002[c]	-0.135[d]	0.008294[e]

Figure 15: Rotational states in O_2^+ including the transition belonging to the highest relative enhancement factor.

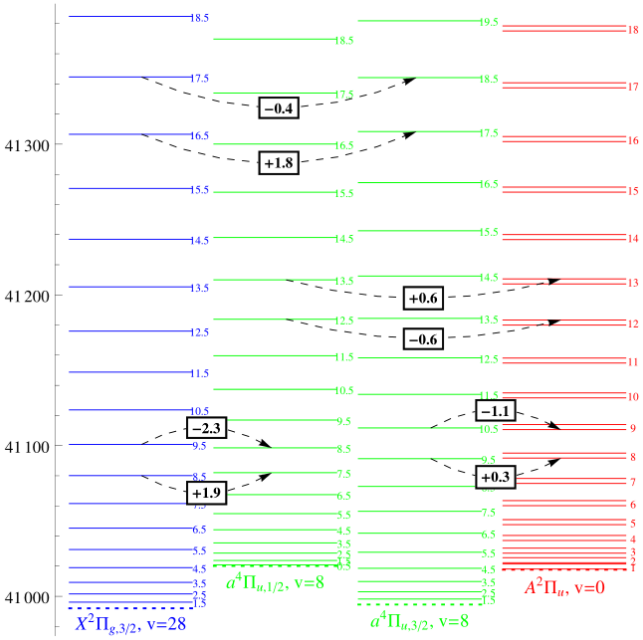

Table 19: Spectroscopic constants of S_2^+. From [96].

constant	$X^2\Pi_g$	$A^2\Pi_u$
T_e (cm^{-1})	0	22354.45
ω_e (cm^{-1})	806.099	552.635
$\omega_e x_e$ (cm^{-1})	3.3971	3.1365
$\omega_e y_e$ (cm^{-1})	-0.00085	-0.00423
B_e (cm^{-1})	0.316974	0.25215
$\alpha_e \times 10^3$ (cm^{-1})	1.7141	1.7307
$\gamma_e \times 10^6$ (cm^{-1})	-3.38	-5.58
$D_e \times 10^6$ (cm^{-1})	0.152	0.161
A_e (cm^{-1})	472.117	12.323
$A_\nu^{(1)}$ (cm^{-1})	-0.467	0.171
$A_\nu^{(2)}$ (cm^{-1})	-0.0252	-0.0223
$A_\nu^{(3)}$ (cm^{-1})	-0.00062	0.00207

Table 20: Spectroscopic constants of $^{12}C_2^+$. From [97].

constant	$X^4\Sigma_g^-$	$B^4\Sigma_u^-$
T_e (cm^{-1})	0	19652.2
ω_e (cm^{-1})	1508.1	805.594
$\omega_e x_e$ (cm^{-1})	12.06	12.69
B_e (cm^{-1})	1.4266	1.5474
α_e (cm^{-1})	0.0176	0.0171
$D_e \times 10^6$ (cm^{-1})	6.361	6.516

15 Appendix G

Table 21: Absolute K_α enhancement factors in cm^{-1} of transitions between low-lying states of SO^+.

States	$X^2\Pi_{1/2}$	$X^2\Pi_{3/2}$	$a^4\Pi_{3/2}$	$a^4\Pi_{1/2}$	$a^4\Pi_{-1/2}$	$A^2\Pi_{1/2}$	$A^2\Pi_{3/2}$
$X^2\Pi_{1/2}$	-	751	173	298	455	251	288
$X^2\Pi_{3/2}$		-	-578	-454	-296	-500	-463
$a^4\Pi_{3/2}$			-	125	282	78	115
$a^4\Pi_{1/2}$				-	157	-47	-9
$a^4\Pi_{-1/2}$					-	-204	-167
$A^2\Pi_{1/2}$						-	37
$A^2\Pi_{3/2}$							-

Table 22: Absolute K_α enhancement factors in cm^{-1} of transitions between low-lying states of O_2^+.

States	$X^2\Pi_{g,1/2}$	$X^2\Pi_{g,3/2}$	$a^4\Pi_{u,1/2}$	$a^4\Pi_{u,3/2}$	$a^4\Pi_{u,5/2}$	$A^2\Pi_{u,1/2}$	$A^2\Pi_{u,3/2}$
$X^2\Pi_{g,1/2}$	-	445	192	83	-17	122	141
$X^2\Pi_{g,3/2}$		-	-253	-362	-462	-321	-304
$a^4\Pi_{u,1/2}$			-	-108	-209	-70	-50
$a^4\Pi_{u,3/2}$				-	-100	38	58
$a^4\Pi_{u,5/2}$					-	138	158
$A^2\Pi_{u,1/2}$						-	20
$A^2\Pi_{u,3/2}$							-

Table 23: Absolute K_α enhancement factors in cm^{-1} of transitions between low-lying states of Cl_2^+.

States	$X^2\Pi_{g,3/2}$	$X^2\Pi_{g,1/2}$	$A^2\Pi_{u,3/2}$	$A^2\Pi_{u,1/2}$	$A^4\Sigma_{u,1/2}$	$A^4\Sigma_{u,3/2}$	$B^2\Delta_{u,5/2}$	$B^2\Delta_{u,3/2}$
$X^2\Pi_{g,3/2}$	-	-1574	-1460	-190	-1038	-890	-920	-577
$X^2\Pi_{g,1/2}$		-	86	1355	509	666	626	970
$a^4\Pi_{u,3/2}$			-	1264	422	570	540	883
$a^4\Pi_{u,1/2}$				-	-847	-699	-729	-386
$A^4\Sigma_{u,1/2}$					-	148	117	461
$A^4\Sigma_{u,1/2}$						-	20	312
$B^2\Delta_{u,5/2}$							-	343
$B^2\Delta_{u,3/2}$								-

Table 24: Absolute K_α enhancement factors in cm^{-1} of transitions between low-lying states of S_2^+.

States	$X^2\Pi_{g,1/2}$	$X^2\Pi_{g,3/2}$	$A^2\Pi_{u,1/2}$	$A^2\Pi_{u,3/2}$
$X^2\Pi_{g,1/2}$	-	987	397	-546
$X^2\Pi_{g,3/2}$		-	-589	-1532
$A^2\Pi_{u,1/2}$			-	-943
$A^4\Pi_{u,3/2}$				-

Table 25: Absolute K_α enhancement factors in cm^{-1} of transitions between low-lying states of C_2^+.

States	$X^4\Sigma_g$	$B^4\Sigma_u$
$X^4\Sigma_g$	-	152
$B^4\Sigma_u$		-

16 Appendix H

Table 26: Relative K_α enhancement factors of transitions between low-lying states of SO^+. Values in brackets indicate the vibrational quantum numbers of the transition.

States	$X^2\Pi_{1/2}$	$X^2\Pi_{3/2}$	$A^4\Pi_{3/2}$	$A^4\Pi_{1/2}$	$A^4\Pi_{-1/2}$	$A^2\Pi_{1/2}$	$A^2\Pi_{3/2}$
$X^2\Pi_{1/2}$	-	no q-d*	890 (30,8)	596 (31,9)	4550 (32,10)	no q-d	no q-d
$X^2\Pi_{3/2}$		-	5780 (25,3)	2270 (26,4)	-1280 (27,5)	no q-d	no q-d
$A^4\Pi_{3/2}$			-	no q-d	no q-d	no q-d	no q-d
$A^4\Pi_{1/2}$				-	no q-d	no q-d	no q-d
$A^4\Pi_{-1/2}$					-	-2040 (8,1)	835 (8,1)
$A^2\Pi_{1/2}$						-	no q-d
$A^2\Pi_{3/2}$							-

* no quasi-degeneracies

Table 27: Relative K_α enhancement factors of transitions between low-lying states of O_2^+. Values in brackets indicate the vibrational quantum numbers of the transition.

States	$X^2\Pi_{g,1/2}$	$X^2\Pi_{g,3/2}$	$a^4\Pi_{u,1/2}$	$a^4\Pi_{u,3/2}$	$a^4\Pi_{u,5/2}$	$A^2\Pi_{u,1/2}$	$A^2\Pi_{u,3/2}$
$X^2\Pi_{g,1/2}$	-	no q-d*	175 (22,1)	no q-d	no q-d	no q-d	no q-d
$X^2\Pi_{g,3/2}$		-	-316 (21,0)	905 (28,8)	no q-d	no q-d	no q-d
$a^4\Pi_{u,1/2}$			-	-no q-d	no q-d	-100(9,1)	-71(9,1)
$a^4\Pi_{u,3/2}$				-	no q-d	123 (9,1)	193 (9,1)
$a^4\Pi_{u,5/2}$					-	no q-d	no q-d
$A^2\Pi_{u,1/2}$						-	no q-d
$A^2\Pi_{u,3/2}$							-

* no quasi-degeneracies

Table 28: Relative K_α enhancement factors of transitions between low-lying states of Cl_2^+. Values in brackets indicate the vibrational quantum numbers of the transition.

States	$X^2\Pi_{g,3/2}$	$X^2\Pi_{g,1/2}$	$A^2\Pi_{u,3/2}$	$A^2\Pi_{u,1/2}$	$A^4\Sigma_{u,1/2}$	$A^4\Sigma_{u,3/2}$	$B^2\Delta_{u,5/2}$	$B^2\Delta_{u,3/2}$
$X^2\Pi_{g,3/2}$	-	no q-d*	-14600 (42,6)	no q-d	-1038000 (42,19)	-2967	no q-d	-721 (42,3)
$X^2\Pi_{g,1/2}$		-	no q-d	no q-d	-5090 (34,8)	no q-d	no q-d	no q-d
$a^4\Pi_{u,3/2}$			-	no q-d	no q-d	no q-d	no q-d	no q-d
$a^4\Pi_{u,1/2}$				-	no q-d	no q-d	no q-d	no q-d
$A^4\Sigma_{u,1/2}$					-	no q-d	no q-d	4610 (18,2)
$A^4\Sigma_{u,3/2}$						-	no q-d	-1040 (24,8)
$B^2\Delta_{u,5/2}$							-	no q-d
$B^2\Delta_{u,3/2}$								-

* no quasi-degeneracies